SKB

TECHNICAL REPORT 91-31

Near field studies within the SKB 91 Project

Hans Widén, Akke Bengtsson, Bertil Grundfelt

Kemakta Consultants AB, Stockholm

June 1991

SVENSK KÄRNBRÄNSLEHANTERING AB
SWEDISH NUCLEAR FUEL AND WASTE MANAGEMENT CO

BOX 5864 S-102 48 STOCKHOLM

TEL 08-665 28 00 TELEX 13108 SKB S
TELEFAX 08-661 57 19

NEAR FIELD STUDIES WITHIN THE SKB91 PROJECT

Hans Widén, Akke Bengtsson, Bertil Grundfelt

Kemakta Consultants AB, Stockholm

June 1991

Near Field Studies within the SKB91 Project

Technical Report

Hans Widén
Akke Bengtsson
Bertil Grundfelt

Kemakta Consultants AB
Stockholm, Sweden

June 1991

ABSTRACT

A number of near field studies was preformed during the early part of the SKB91 project. This report summaries this work and includes:

- Simulation of the steady state release from the near field with different time for canister penetration.

- Simulation of the release from a repository with 5300 canisters with different penetration times for different parts of the canisters due to manufacturing error, glaciations, inner over pressure and corrosion.

- Calculation with a numerical model of the transient release of the instantaneously dissolvable species and the effect of different boundary conditions both at the canister/bentonite and the bentonite/rock interface.

- Description of the implementation of a resistance network model for the calculation of the steady state transport resistances in the different pathways from the canisters

- Comparison of two analytical models for the calculation of the release of the instantaneously dissolvable species.

CONTENTS

1 INTRODUCTION AND BACKGROUND

The KBS-3 concept for disposal of high level radioactive waste consists of a number of independent barriers. The low solubility of the waste matrix, the copper canisters surrounding the waste, the bentonite clay outside the canisters, and the 500 meters of rock above the repository. This report consist of a number of studies concerning the near field barriers, i.e. studies of the release from the canisters into the rock just outside the bentonite clay that were performed as background to the SKB91 safety assessment project. The different parts are:

- Simulation of different scenarios for canister breakthrough time cased by, manufacturing error, glaciations, inner over pressusre and corrosion calculated with the NEAR21 (TULLGARN) code.

- Study of the effect of diffusion geometry on the transient transport rate of the inventory of readily dissolvable species through the bentonite backfill calculated with the Integrated Finite Difference code TRUMP.

- The implementation of a new resistance network model into TULLGARN for calculation of the steady state diffusion transport rates from the near field.

- Comparison between two codes describing simplified geometric models for the transient release of the readily dissolvable species.

2 DESCRIPTION OF THE MODEL

The NEAR21 code that was used in this study is described in detail in (Norman and Kjellbert). The model computes the steady state migration rates of radionuclides and decay chains of radionuclides from the near field of KBS-3 canisters. Canister corrosion, diffusive transport, fuel matrix dissolution, solubility limitations at reducing and oxidizing conditions, fast washout of instantly released part of the inventory and chain decay are all taken into account.

The model can also be used to calculate the release from more than one canister and α-radiolysis induced dissolution rate can be modelled. It is assumed that steady-state conditions prevail for both the inward transport of corrodants and for the outward transport of radionuclides. The time for canister penetration can also be set explicitly to occur at an earlier time than if determined by the corrosion rate. Figure 2-1 shows the modelled system.

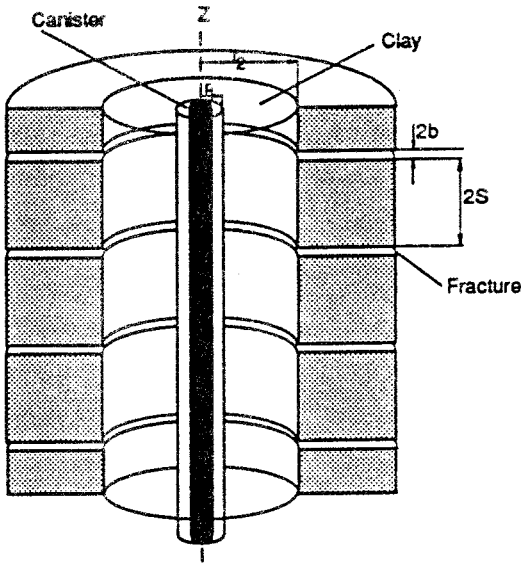

Figure 2-1. The modelled system consists of a KBS-3-type canister surrounded by bentonite clay with fissured rock outside the buffer material.

For the calculations in this Chapter the mass transfer resistance caused by the limited area of the penetration hole is neglected so that when the canister is penetrated, the whole fuel surface is assumed to be available for the groundwater attack.

2.1 PERFORMED CALCULATIONS

The six base cases describing the release from a single canister has identical input data except for the time when the copper canister is penetrated is defined in Table 2-1. All time references are calculated from year 2035.

Table 2-1. Definition of the six base cases

Case number	penetration time [years]	reason for failure
1	100	manufacturing error
2	25000	glaciation
3	65000	glaciation
4	125000	glaciation
5	10^6	inner over pressure
6	corrosion dependent	corrosion

In order to simulate the near-field release from a full repository according to the KBS-3 concept a number of combination cases were designed. These combination cases J to R consists of a total of 5300 canisters with different times for canister penetration according to base cases 1-6. The α-radiolysis induced dissolution model was used for all calculations described in this report. The composition of the combination cases are shown in Table 2-2. The results are plotted as Becquerel/year as a function of time for the nuclides that were considered being the most important. Dose calculations were also performed as if no far field barriers existed, i.e. that the release from the near field is released directly in the biosphere. The results of the dose calculations together with the results from the solubility limitation model is available in (Widén et al., 1990).

Table 2-2. Definition of combination cases given as % of canisters penetrated according to respective base case (the total number of canisters in the repository is 5300). For cases O and P the actual number of canisters are given.

Base case	% 1	% 2	% 3	% 4	% 5	% 6
comb. case						
J	1	10	20	30	0	39
K	1	10	10	10	0	69
L	1	30	20	10	0	39
M	10	10	10	10	0	60
N	1	10	10	10	69	0
O	1	0	0	0	5299	0
P	1	0	0	0	0	5299
Q	1	0	0	0	99	0
R	1	0	0	0	0	99

2.2 DATA USED

The solubilities of the nuclides are given in Table 2-3 and the other input data are compiled in Table 2-4. Note that the data in these tables in several instances are different than the central case in SKB91 because the calculations described here were performed before any "official" SKB91 input data had been defined. The solubilities used are for salt water beacase tthe SKB91 project concerns the Finnsjön site were the water has a high salt content.

Table 2-3. Solubility (mol/l) used for oxidizing and reducing conditions for salt water. Shown are also the solid phase limiting the solubility and the dominating species in the solution.

	ox.	dom. spec.	red.	dom. spec.
U	$3 \cdot 10^{-5}$ Schoepite	$UO_2(CO_3)_2^{2-}$ $UO_2(CO_3)_3^{4-}$	$2 \cdot 10^{-7}$ Uranite	$U(OH)_4$
Pu	$3 \cdot 10^{-9}$ $Pu(OH)_4$	PuO_2^+	$5 \cdot 10^{-8}$ $Pu(OH)_4$	Pu^{3+} $PuSO_4^+$
Np	$4 \cdot 10^{-4}$ $NaNpO_2CO_3$	NpO_2^+ NpO_2Cl	$4 \cdot 10^{-7}$ $Np(OH)_4$	$Np(OH)_5^-$

Table 2-3. Continued.

Am	$6 \cdot 10^{-8}$ $AmOHCO_3$	$AmCO_3^+$ Am^{3+}	$5 \cdot 10^{-8}$ $AmOHCO_3$	$AmCO_3^+$ Am^{3+}
Th	$2 \cdot 10^{-10}$ ThO_2	$Th(OH)_4$	$2 \cdot 10^{-10}$ ThO_2	$Th(OH)_4$
Ra	$2 \cdot 10^{-7}$ $RaSO_4$	Ra^{2+}	$2 \cdot 10^{-7}$ $RaSO_4^+$	Ra^{2+}
Sn	$2 \cdot 10^{-8}$ SnO_2	$Sn(OH)_4$	$2 \cdot 10^{-8}$ SnO_2	$Sn(OH)_4$
Tc	High	TcO_4^-	$1 \cdot 10^{-8}$ TcO_2	$TcO(OH)_2$

Table 2-4. Input data used for the calculations

Horizontal Darcy velocity	$1 \cdot 10^{-4}$	($m^3/m^2 \cdot y$)
Vertical groundwater flowrate	0	($m^3/m^2 \cdot y$)
Half fissure width i near field	$5 \cdot 10^{-5}$	(m)
Effective diffusivity in clay buffer	$1.3 \cdot 10^{-3}$	(m^2/y)
Diffusivity in flowing water	$6.0 \cdot 10^{-2}$	(m^2/y)
Fissure spacing outside buffer	1.0	(m)
Inner diameter of canister	0.6	(m)
Outer diameter of canister	0.8	(m)
Diameter of deposition hole	1.5	(m)
Porosity of buffer	0.2	(-)
Density of buffer	2100	(kg/m^3)
sulphide concentration	0.015	(mol/m^3)
G value for α-induced oxidation/ dissolution of UO_2 in molecules/100 eV	$2.5.10^{-5}$	
Pitting factor	2	(-)

The radionuclides that were included in the calculations were ^{14}C, ^{93}Zr, ^{99}Tc, ^{126}Sn, ^{129}I, ^{135}Cs and the decay chains that are shown in Figure 2-2.

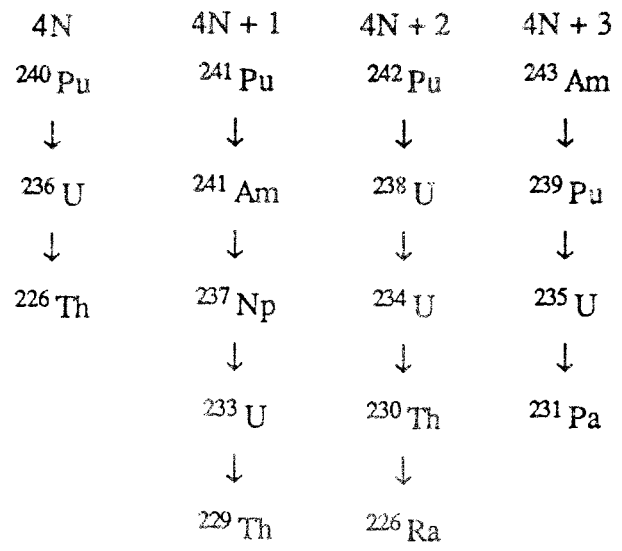

Figure 2-2. The nuclides in the decay chains that was studied. Not all of the nuclides are shown in the plots. The nuclides that give a very small contribution to the total dose were left out.

2.3 RELEASE CURVES FOR THE BASE CASES

The results from the base cases 1 to 6 are given in Appendix 1 and as an example case 1 is shown in Figure 2-3.

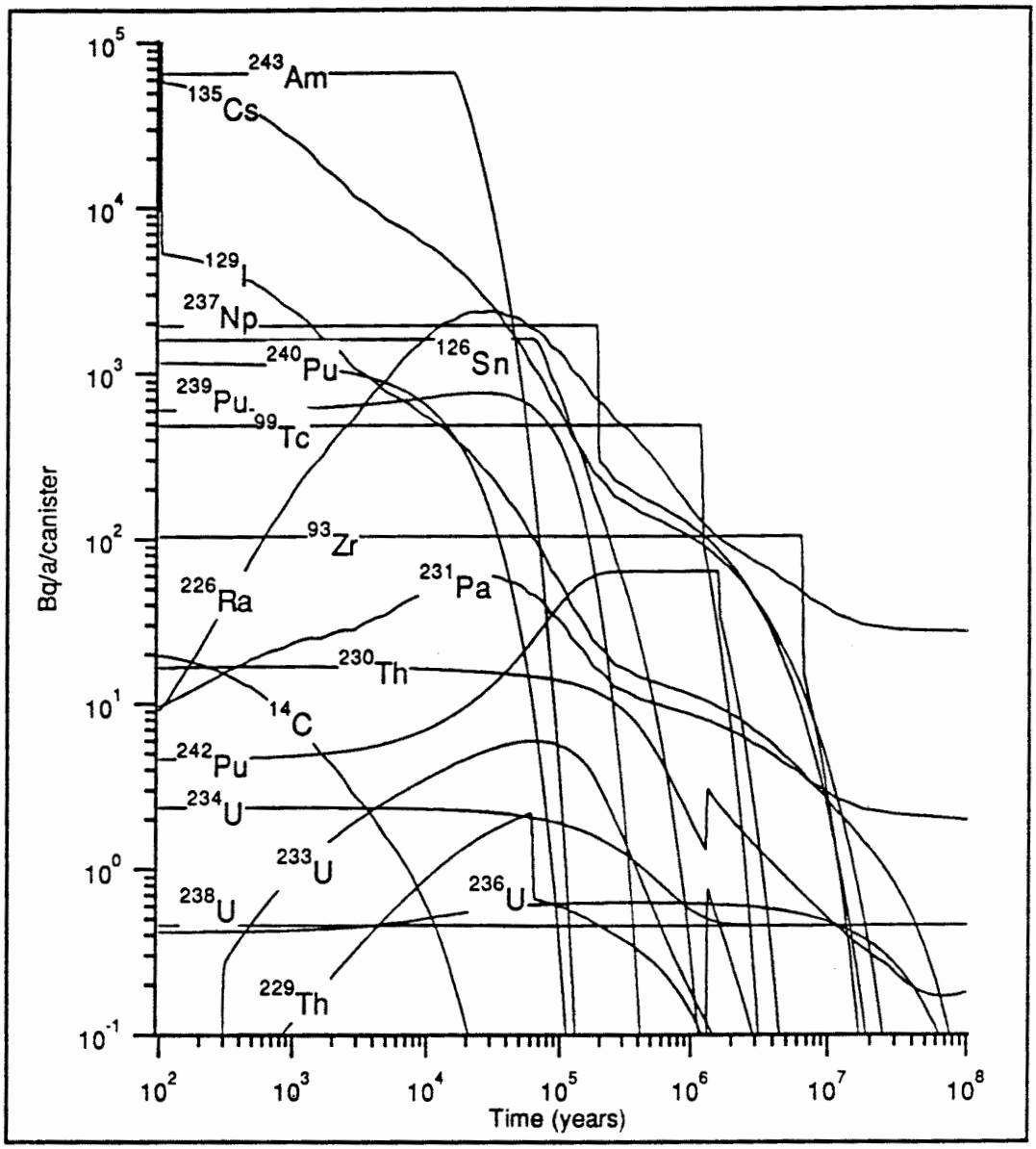

Figure 2-3. Result for case 1 calculated with α-radiolysis induced dissolution model for one canister

2.4 RELEASE CURVES FOR THE COMBINATION CASES

The results from the combination cases J to R are given in Appendix 1, as an example case J is shown below in Figure 2-4.

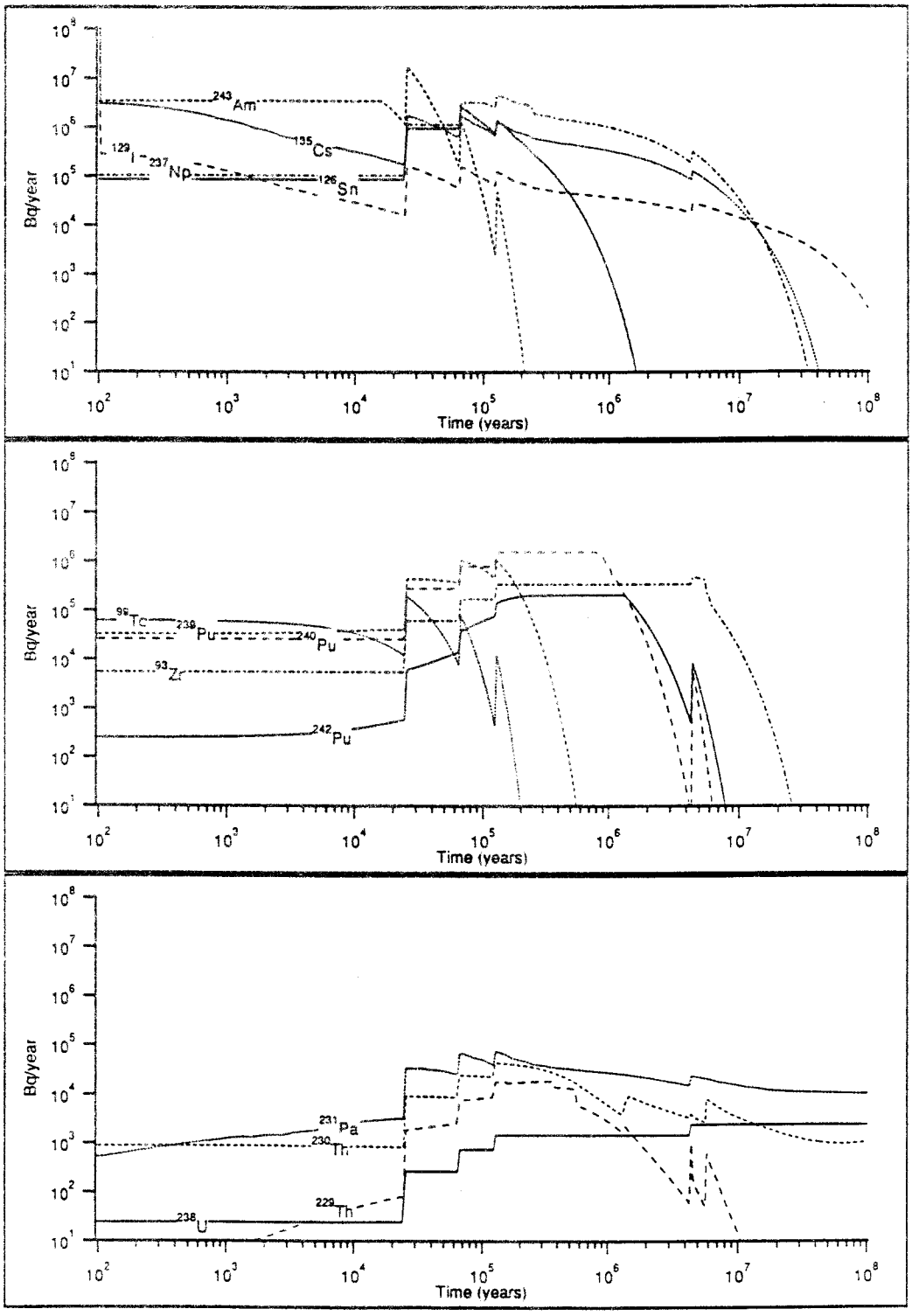

Figure 2-4. Result for case J calculated with α-radiolysis induced dissolution model for a total of 5300 canisters.

The highest release rates are for ^{243}Am, ^{135}Cs, ^{129}I and ^{237}Np when measured in Bq/year. When converison to dose was performed to get an estimate on the contributions of the idividual nuclides to the total dose ^{231}Pa together with ^{237}Np gave the largest contribution for all combination cases.

The dose calculation below are based on the release from the near field as if no far field barriers existed, the dose conversion factors are taken from (Bergstöm and Nordlinder, 1990). Table 2-5 shows a compilation of the results from the dose calculations for the combination cases J to R.The column "largest contribution" shows the nuclide that has the highest max-value, not necessarily at the same time as when the total dose has its maximum. The part of ^{129}I and ^{135}Cs that is available for instantaneous dissolution is not taken into account for this table because this is not well handled by the TULLGARN code at present. In Appendix 3 two models for this type of calculation is compared.

Table 2-5. Compilation of results for combination cases J to R. Maximum total dose and the nuclide giving the largest contribution to the total dose.

Case	maximum total Sv/year	largest contribution
J	$4.4 \cdot 10^{-5}$	^{237}Np
K	$2.6 \cdot 10^{-5}$	^{237}Np
L	$6.2 \cdot 10^{-5}$	^{231}Pa
M	$3.6 \cdot 10^{-5}$	^{237}Np
N	$2.6 \cdot 10^{-5}$	^{237}Np
O	$1.7 \cdot 10^{-5}$	^{231}Pa
P	$5.8 \cdot 10^{-6}$	^{231}Pa
Q	$1.7 \cdot 10^{-5}$	^{231}Pa
R	$5.8 \cdot 10^{-6}$	^{231}Pa

3 TRANSIENT RELEASE OF THE GAP INVENTORY

The waste canisters in a KBS-3 repository for spent nuclear fuel are embedded in bentonite clay. In this study the transient release rates past the bentonite barrier of a fixed amount of initial clad-gap activity of high solubility is calculated.

The effect of restricting the area of the canister surface/bentonite and bentonite/rock interface is also studied. On the outer side of the bentonite barrier the bentonite/rock interface area could be limited to the openings of fracture planes in the surrounding rock. A hole in the copper canister could also give a limited boundary surface area to the bentonite barrier.

Boundary surface area restrictions such as these means a decrease in the effective area for diffusion into and from the bentonite giving a reduced transport rate overall. In this study all the four combinations of reduced boundary surface or full area on the inner- and outer side of the bentonite barrier are compared.

3.1 CASE DESCRIPTION

The radial outwards diffusion through the cylindrical mantle of the bentonite barrier is simplified to diffusion through a slab of 0.35 m thickness. The area of the slab is limited to 1 x 1 m. The hole in the canister wall is placed in the middle of the 1 m^2 surface. A maximum area of 5 mm^2 for the initial penetration (derived from the maximum area that a defect in the canister/lid weld could have and still have a chance of passing the materials inspection.) In the cases with diffusion to a fracture plane in the host rock on the outer side of the barrier, this fracture plane is assumed to be opposite the hole in the canister. A fracture plane with a width of 0.1 mm is assumed. Because of symmetry actually only a quarter of the 1 m^2 slab needs to be modelled. (See Figure 3-1). The materials data for the bentonite are shown in Table 3-1.

Table 3-1. Material data for the bentonite.

Effective diffusivity, D_e	$1.3 \cdot 10^{-3}$ m^2/a
Porosity, ep	0.2 m^3/m^3
Density, ρ	2100 kg/m^3

Using:

$$V_{eff} = V\left(\varepsilon_p + \rho K_d\right) \tag{3-1}$$

and the volumes we could calculate the effective capacity V_{eff} of the clad-gap volume and the bentonite, including the effect of sorption, see Table 3-2.

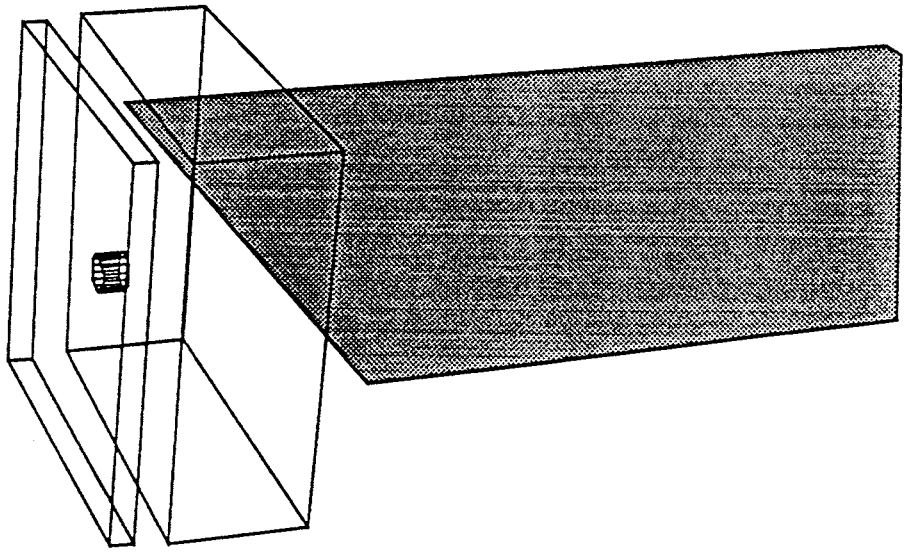

Figure 3-1 Geometry for simplified model of diffusion through the bentonite surrounding a KBS-3 type canister.

Table 3-2. Effective capacities corresponding to a 1x1 m slab of bentonite.

	Effective capacity [m^3]
Clad gap	$9.1 \cdot 10^{-3}$
Bentonite (K_d = 0)	$70 \cdot 10^{-3}$
Bentonite (K_d = 0.05)	36.8

The initial conditions are zero concentration everywhere in the bentonite barrier and a concentration giving an initial amount of 1.0 arbitrary mass units in a water volume corresponding to the clad-gap volume. The fuel/canister clad-gap volume

is supposed to be 0.02 m^3/ 2.2 m^2 of bentonite barrier which means that it is modelled as 9.1 mm thick. This means that the initial concentration in the water in the gap volume will be 110 moles/m^3. If the initial inventory is set to 1 mol and 1 m^2 of the bentonite surface is modelled.

The boundary condition on the outlet side is zero concentration.

3.2 INITIAL ESTIMATES OF TIME SCALE AND CONCENTRATIONS

To judge the correctness of the numerical calculations of the instationary transport some preliminary calculations have been made. Also a rough comparison of the four possible combinations of boundary conditions is presented.

The barrier function of the bentonite barrier is profoundly affected by a decrease in the interface area to the boundary condition. Most of the concentration drop then takes place in a small volume of the bentonite adjacent to the boundary condition. If the bentonite/boundary condition interface area is sufficiently small this volume will be so small that the time to establish steady state conditions in it will be very short compared to the whole barrier. The total mass transfer resistance will then be dominated by the resistance in this volume which could be calculated from steady state conditions.

A steady state transport rate through a barrier could be expressed as the product of an equivalent water flow rate q_{eq}(m^3/a) and the concentration difference across the barrier.

$$Q = q_{eq}\Delta C \tag{3-2}$$

The equivalent water flow rate for a layer of bentonite close to the 5 mm^2 hole in the canister could be calculated for a hollow spherical shell using the equations shown in Section 3.2.1. The equivalent water flow rate is shown in Figure 3-2 as a function of the thickness of the shell for a hollow half sphere with an inner surface area = 5 mm^2. Actually $1/q_{eq}$ is plotted for convenience which could be thought of as a mass transfer resistance.

The same kind of calculation for a 0.1 mm slit, 1 m long could be made using the equations for a cylindrical shell in Section 3.2.1. The mass transfer resistance as a function of the thickness of the cylindrical shell is shown in Figure 3-3.

3.2.1 Mass transfer resistance at steady state for a hollow spherical shell

The concentration profile in a spherical shell with inner radius a and outer radius b with the concentrations C_a at $r=a$ and C_b at $r=b$ is given by:

$$C(r) = \frac{aC_a}{r} + \frac{\left(bC_b - aC_a\right)\left(r-a\right)}{r\left(b-a\right)} \tag{3-3}$$

(Adaption of Equation 1 at page 246 of Carslaw&Jaeger for t→∞)
If $C_a = C_0$ and $C_b = 0$, the diffusive transport rate through a conical sector with a solid angle of θ steradians is given by:

$$Q = -r^2\theta D_e\frac{\partial C}{\partial r} = \theta r^2 D_e C_0 \frac{ab}{r^2\left(b-a\right)} \tag{3-4}$$

If we choose to express the diffusive transport rate at steady state in the same way as for transport across a boundary layer with an area A, a mass transfer coefficient α (m/s) and a concentration difference ΔC, we could write the transport rate in an alternative way as:

$$Q = A\alpha\Delta C \tag{3-5}$$

Identification with Equation 3-4 gives us:

$$\alpha = D_e\frac{ab}{r^2\left(b-a\right)} \tag{3-6}$$

and:

$$A = r^2\theta \tag{3-7}$$

The product of A and α could conveniently be thought of as an equivalent water flow rate q_{eq} (m^3/s) which multiplied by the concentration difference over the layer (C_0–0) gives the transport rate past the cylindrical shell.

3.2.2 Mass transfer resistance at steady state of a hollow cylinder

The mass transfer resistance at steady state for the part of the bentonite closest to the intersection of the external surface of the bentonite barrier and a fracture plane in the host rock is calculated in the following way:

The inward mass transport rate through a wedge of a hollow cylinder with centre angle ϕ (radians), length l, inner radius a, outer radius b with a concentration C_0 outside and zero inside will be:

$$Q = \frac{r\phi l D_e C_0}{r \ln\left(\frac{a}{b}\right)} \tag{3-8}$$

If we choose to express the diffusive transport rate at steady state in the same way as for transport across a boundary layer with an area A, a mass transfer coefficient α (m/s) and a concentration difference ΔC, we could write the transport rate in an alternative way as:

$$Q = A\alpha\Delta C \tag{3-9}$$

Identification with Equation 3-8 will give:

$$\alpha = \frac{D_e}{r \ln\left(\frac{a}{b}\right)} \tag{3-10}$$

and:

$$A = r\phi l \tag{3-11}$$

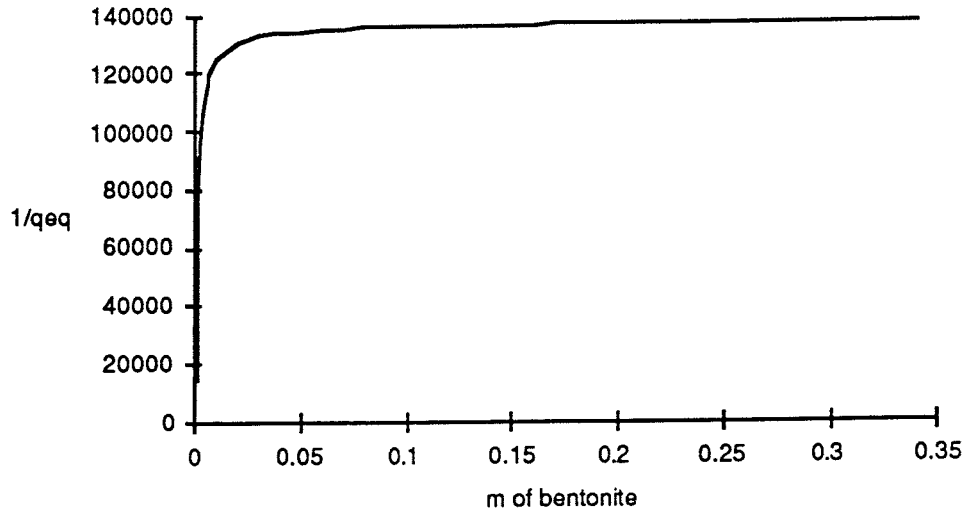

Figure 3-2. Mass transfer resistance at steady state for the bentonite adjacent to a 5 mm^2 hole.

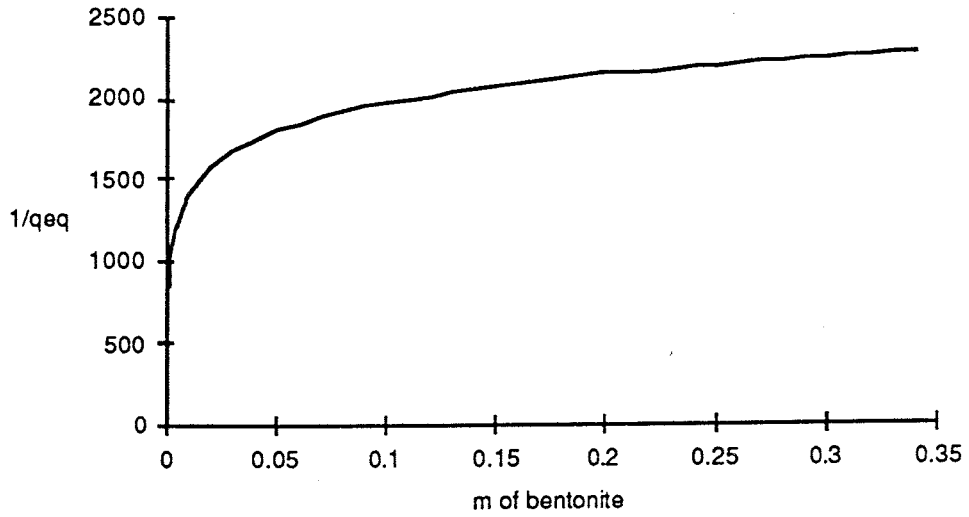

Figure 3-3. Mass transfer resistance at steady state for the bentonite adjacent to a 1 m long slit with a width of 0.1 mm.

As can be seen from Figures 3-2 and 3-3 the mass transfer resistance at steady state does not increase very much going beyond the first cm of bentonite both for the hole and the slit. The mass transfer resistance of the hole is also much larger

than that of the slit. This does not necessarily mean that the slit does not have a significant effect even in combination with the hole. Particularly for K_d-values above zero the sorption capacity of the bentonite barrier (Table 3-2) will limit the maximum concentration drop over the last cm of bentonite (but not over the first cm).

Let us show this by calculating the stationary state transport rates past the cm of bentonite closest to the hole and the slit. We assume that the initial amount of material is uniformly distributed over the upstream volumes and zero concentration downstream.

For the hole the upstream concentration would be the initial amount of material divided by the gap volume. For the slit the concentration on the upstream side will be the initial amount divided by the sum of the individual capacity (in m^3) of the gap volume and the bentonite, including the effect of sorption in the bentonite. Table 3-3 shows the so calculated transport rates for $K_d = 0.0$ and $K_d = 0.05$ using the Equations shown in Sections 3.2.1 and 3.2.2.

Table 3-3. Maximum fractional transport rate at steady state past a 1 cm shell of bentonite. Concentration corrected for sorption in a 1*1 m slab of bentonite, 0.35 m thick

	ΔC_{max}	Q_{max} [a^{-1}]
$K_d = 0$, hole	110	$8.8 \cdot 10^{-4}$
$K_d = 0$, slit	12.6	$8.9 \cdot 10^{-3}$
$K_d = 0.05$, hole	110	$8.8 \cdot 10^{-4}$
$K_d = 0.05$, slit	$27.2 \cdot 10^{-3}$	$1.9 \cdot 10^{-5}$

3.3 NUMERICAL CALCULATION, DISCRETISATION

A slab of 0.5 x 0.5 m of bentonite, 0.35 m thick is discretized into 20 approximately equal divisions going from the inside outwards and 15x15 divisions in the other two directions. Because of symmetry this volume can represent one quarter of the 1*1*0.35 m slab in Figure 3-1.

The normal way to discretise a volume for a finite-difference calculation means that small size geometrical features needs a discretisation of the same scale to be modelled faithfully. As there is a definite limit in how large the difference in size between two connected node volumes could be. The number of nodes could become very large if the smallest modelled features are much smaller than the whole modelled volume, particularly for a 3-D model. It is in this case not

practical to model the parts of the bentonite barrier closest to the hole in the canister and the fracture in the host rock with nodes of the same sizes as the boundary interface areas. The node volumes directly in contact with the concentration boundary conditions are thus removed. The nodes previously connected to them are instead connected directly to the concentration boundary condition with a mass transfer resistance equal to the mass transfer resistance at steady state of the excluded nodes. The volumes so replaced are:

- on the input side a cube of 1x1x1 cm with the center of the hole in the canister wall at one corner. The mass transfer resistance at steady state is calculated as for a cone with a solid angle of $\pi/2$ steradians out of a hollow sphere with 5.0/4 mm^2 inner area (r_i=0.89 mm) and an outer area of 3x1.0x1.0 cm^2 (r_o=1.38 cm).

- on the outlet side the resistance is calculated as for a half cylinder. An inner area of a half cylinder giving the same area per unit length as the fracture opening (0.5 mm) gives an inner radius of 0.0318 mm. The outer surface area per unit length of the $\pi/2$ sector of the cylinder is modelled as the sum of the two 1 cm wide interface areas to the adjacent nodes giving an outer radius of 1.27 cm.

The capacity of the excluded volumes are so small compared to the whole volume that leaving them out (except for the mass transfer resistance of course) does not make any discernible difference in the release rates.

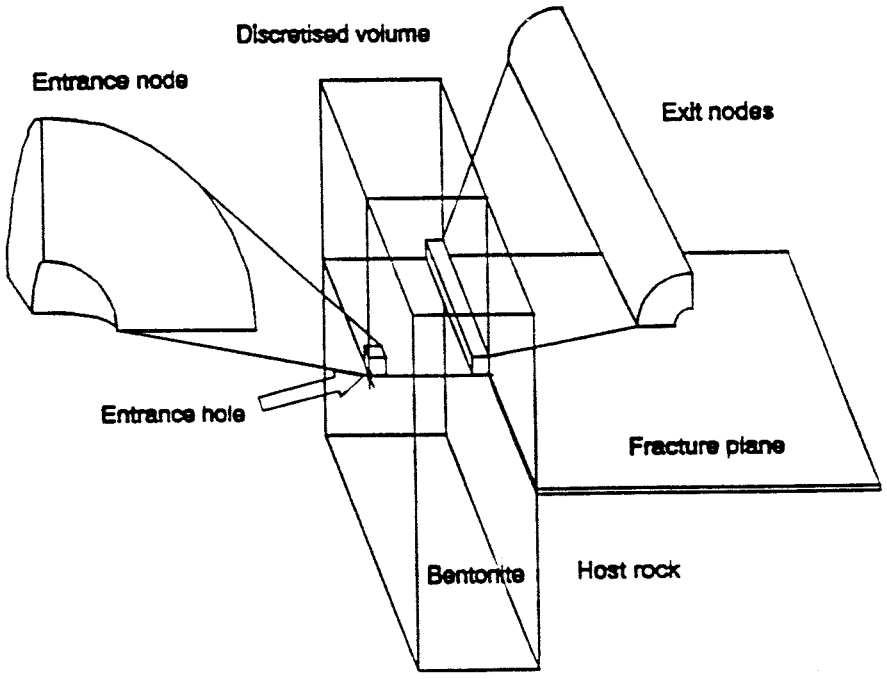

Figure 3-4. Some details of the discretisation for the numerical modelling.

3.4 RESULTS

The fractional release rates of I-129, Cs-135 and Cs-137 corrected for radioactive decay are shown in Figures 3-4 to 3-6 for the different combinations of boundary conditions. The combinations are described in Table 3-4.

Table 3-4. Case descriptions for the numerical calculations

Case	Description
A	Diffusion from 1 m^2 surface to a 0.1 mm slit
B	Diffusion from 5 mm^2 hole to a 1 m^2 surface
C	Diffusion from 5 mm^2 hole to a 0.1 mm slit
D	Diffusion from 1 m^2 surface to a 1 m^2 surface

The results are maybe somewhat unexpected. For instance, the relative importance of boundary area restrictions before or after the bentonite barrier are reversed when there is any appreciable sorption capacity in the bentonite. The decrease in diffusion area is certainly larger for the 5 mm^2 hole than for the 1 m long 0.1 mm slit and for $K_d = 0$ the release rate at the end of the bentonite barrier is lowest for the two cases with the hole. For $K_d = 0.05$ the two cases with the slit give the lowest overall release rates except for Cs-137 where the early arrival in the Full area - slit case let a larger fraction through before radioactive decay has taken its toll. The higher transport capacity of the slit compared to the hole is for $K_d = 0.05$ more than well compensated by a lower possible concentration gradient over the last cm up to the slit because of substantial sorption of the initial amount of migrating substance before reaching the slit. The total effective capacity of the gap volume plus the bentonite (assuming total saturation of the bentonite) is about a factor 450 larger with $K_d = 0.05$ than with $K_d = 0.0$. (Compare with the maximum possible release rates calculated in Table 3-3).

The fraction of initial gap activity annually released from the bentonite as a function of time is shown in Figures 3-8 and 3-9 for $K_d = 0.0$ and 0.05. The data for these two Figures are calculated by integration of the fractional release rates without correction for radioactive decay.

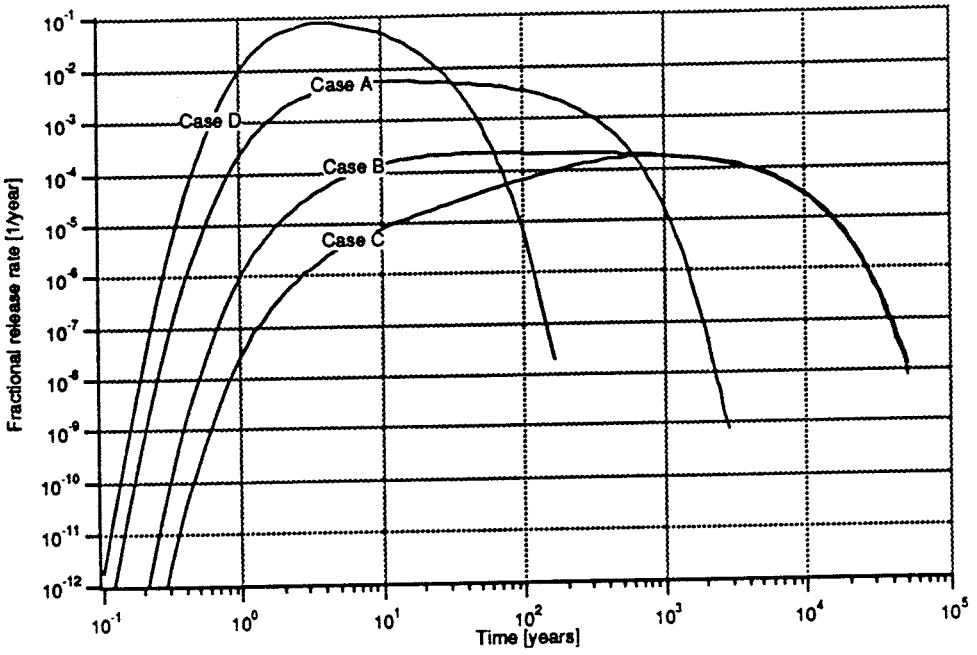

Figure 3-5. Fractional release rate of I-129.

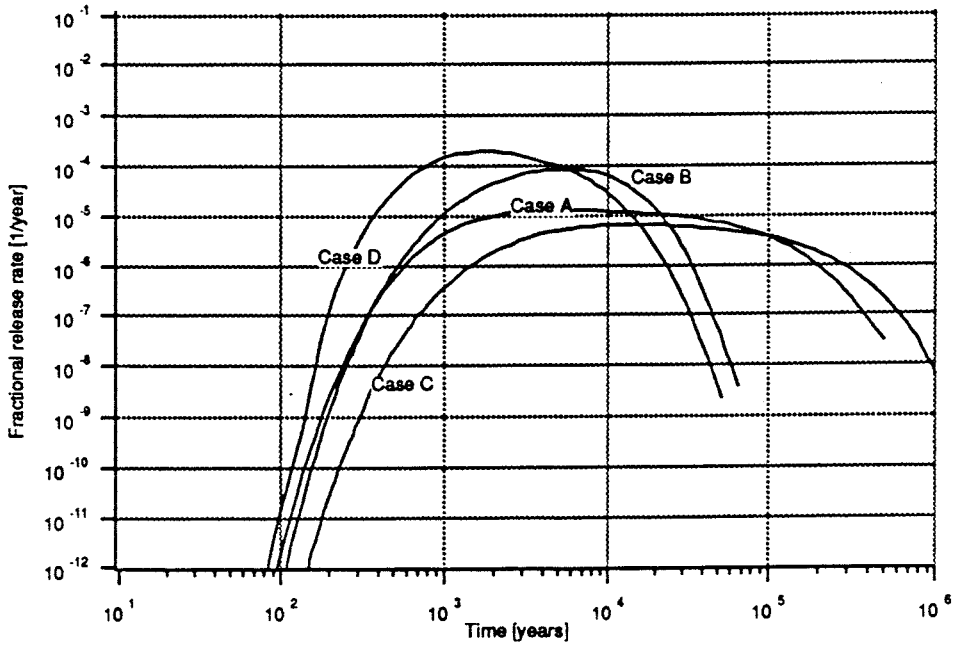

Figure 3-6. Fractional release rate of Cs-135.

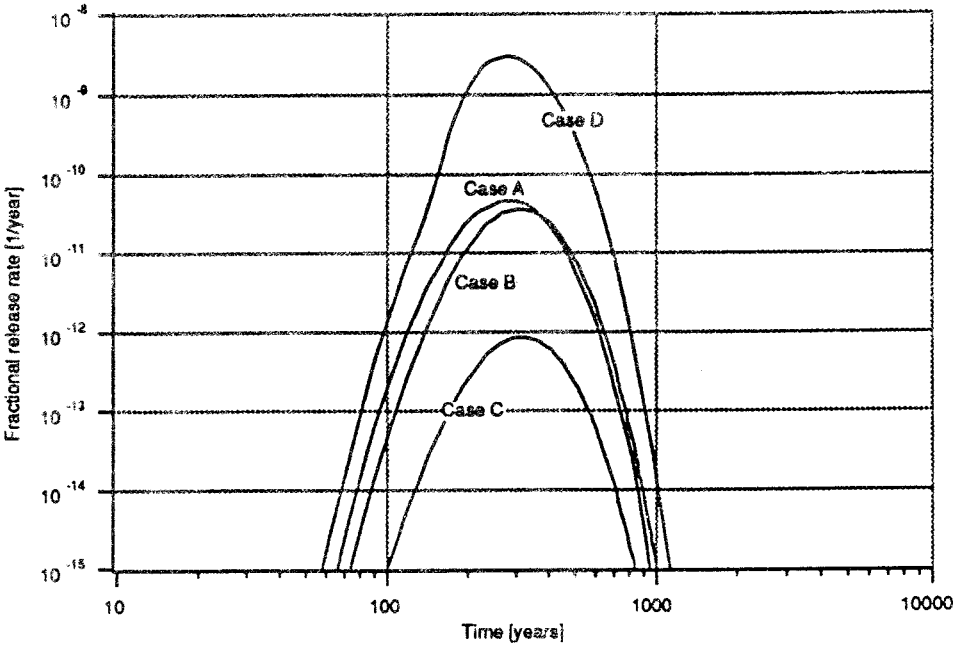

Figure 3-7. Fractional release rate of Cs-137.

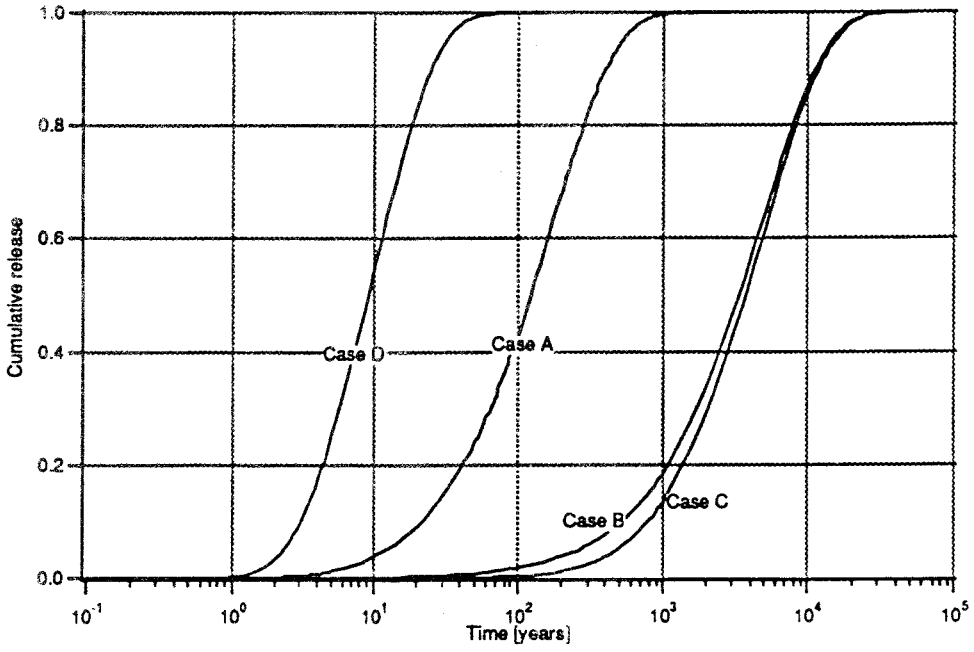

Figure 3-8. Released fraction with $K_d = 0$.

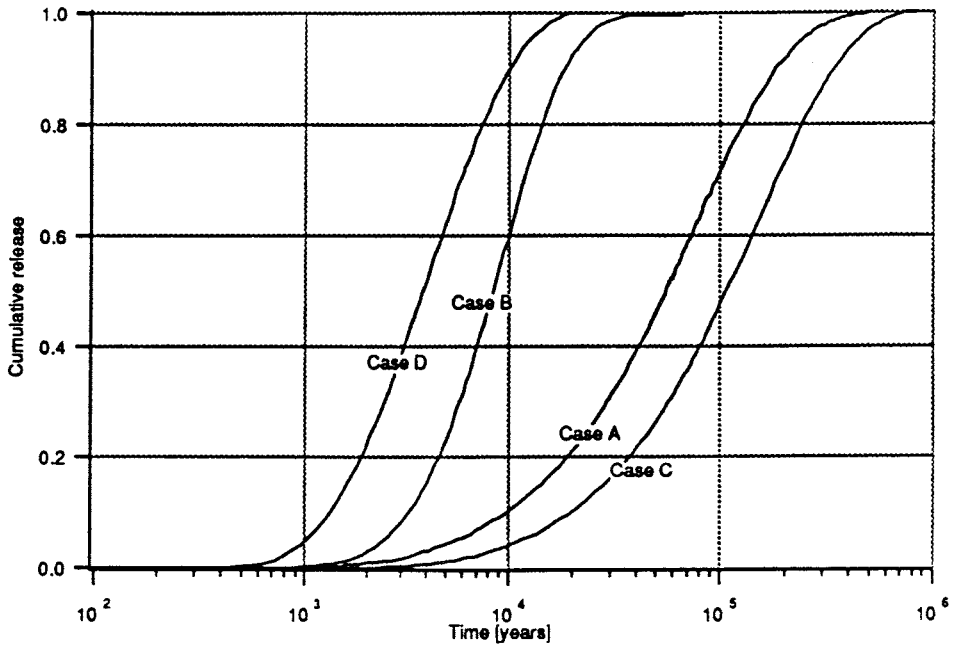

Figure 3-9. Released fraction with K_d = 0.05.

3.5 DISCUSSION

Despite the deliberately very simple geometry modelled, most of the results are valid even for the cylindrical geometry of a real bentonite barrier.

This holds particularly for the cases where there is no restrictions of the outer boundary surface area. As was shown in the analytical calculation, only the bentonite in the immediate vicinity of the hole in the canister will affect the maximum release rate. The time scale of the instationary diffusion through the bentonite will for all practical purposes be set by the thickness and diffusivity of the bentonite barrier and the sorption in the bentonite. Therefore the actual total bentonite area utilized will not make much difference.

The treatment of the intersection between the bentonite and a fracture plane in the host rock is more schematic. The length of the bentonite/fracture interface is 1 m in the present study. This is about one third of the circumference of the outer surface of the bentonite barrier.

Starting with the case with the whole inner surface of the bentonite accessible as boundary surface, the effect on the maximum release rate of adding more bentonite/fracture interface area on the outer side would be additive as long as the fracture width and total bentonite volume is constant. The time scale of the concentration profile build up phase would not be affected.

4 IMPLEMENTATION OF RESISTANCE NETWORK MODEL

It was decided that the near field model to be used in SKB91 should be modified to incorporate the phenomenon that bentonite can penetrate into the fractures in the rock surrounding the deposition holes of the copper canisters. The changes in the code should be based on (Nilson, et al., 1991). The transport path vertically to the disturbed zone was also to be modelled by the simple assumption that the penetration hole in a canister is located at the lid of a canister and that the resistance once the radionuclides has diffused up to the disturbed zone is negligible.

4.1 DESCRIPTION OF THE RESISTANCE NETWORK MODEL

Most of the base for this model is described in (Norman and Kjellbert , Nilson, et al., 1991) with some additions:

- The model can account for more than one fracture/deposition hole.
- The resistance up to the "disturbed zone" in the tunnel above the deposition hole is included.
- The resistance imposed by the limited area available for diffusion out from a canister penetrated by a small hole is also included.

The geometry and the equivalent resistance network of the modelled system is shown in Figures 4-1 and 4-2.

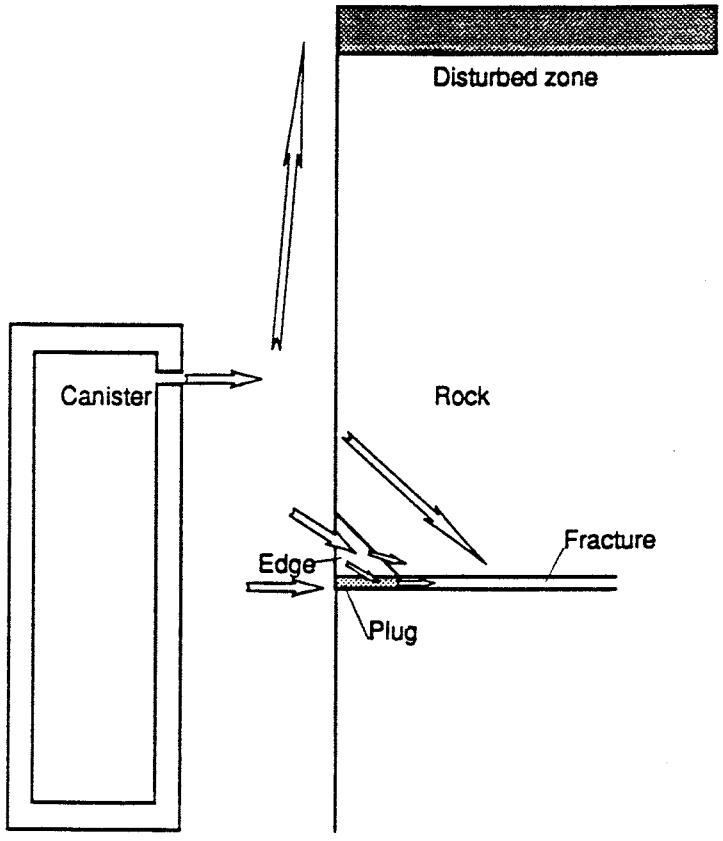

Figure 4-1. Geometry of the modelled system with the different transport pathways drawn as arrows.

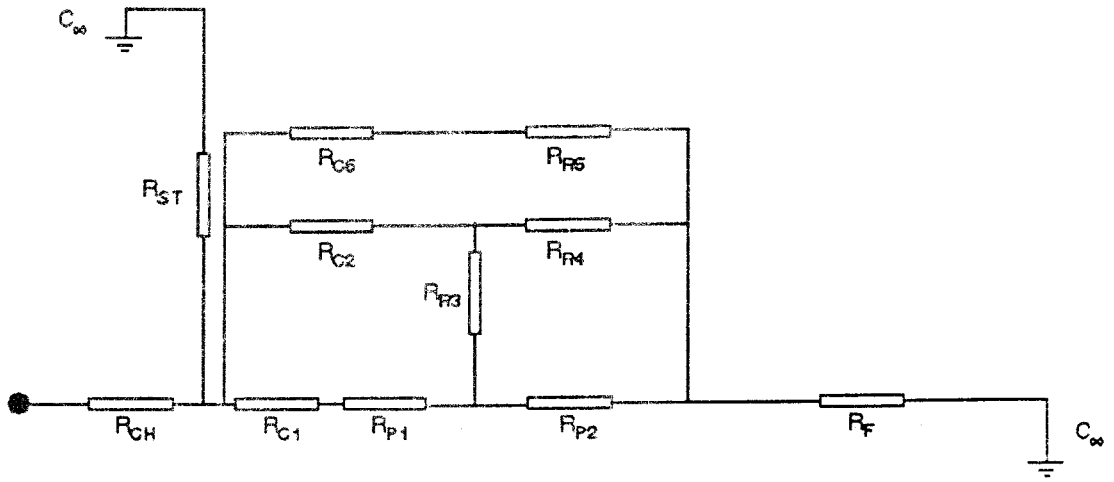

Figure 4-2. Description of the resistances and their connections with only one fracture in the deposition hole.

The Equations on which the code is based are described below.

The resistance caused by the hole in the canister, R_{CH}

$$R_{CH} = \frac{1}{\pi \lambda D_C} \tag{4-1}$$

where λ = the diameter of the penetration hole [m]
D_C = the effective diffusivity in the clay [m^2/a]

The resistance up to the "disturbed zone", R_{ST}

$$R_{ST} = \frac{L_{ST}}{A_{Dep} D_C} \tag{4-2}$$

where L_{ST} = distance from the penetration hole up to the disturbed zone [m]
A_{Dep} = the area of the deposition hole [m^2]

It is assumed that the penetration hole is located near the top of the canister so that A_{Dep} can be taken to be the unrestricted area of the deposition hole.

The resistance in the clay to the fracture opening, R_{C1}

$$R_{C1} = \frac{F\left(a, \beta + \frac{\nu}{2}\right)}{A_{Fract} D_C}$$
$$A_{Fract} = \pi d_h \delta \qquad (4\text{-}3, 4)$$

where a = bentonite thickness[m]

$\beta = 0$ [m]

$\nu = \frac{\delta}{2}$ = half of the fracture width δ [m]

d_h = the diameter of the deposition hole [m]

$F\left(a, \beta + \frac{\nu}{2}\right)$ is defined in Equation 4-16.

The resistance in the clay to the fracture opening, R_{C2}

$$R_{C2} = \frac{F\left(a, \beta + \frac{\nu}{2}\right)}{A_{Edge} D_C}$$
$$A_{Edge} = \pi d_h \sigma \qquad (4\text{-}5, 6)$$

where

a = bentonite thickness[m]

$\beta = \frac{\delta}{2}$ = half of the fracture width [m]

$\nu = \sigma$ =the plug length [m]

The resistance in the clay to the rock, R_{C6}

$$R_{C6} = \frac{F\left(a, \beta + \frac{\nu}{2}\right)}{A_{Rock} D_C}$$
$$A_{Rock} = \pi d_h (S - \delta - 2\sigma) \qquad (4\text{-}7, 8)$$

$\beta = \frac{\delta}{2} + \sigma$

$\nu = S - \delta - 2\sigma$ [m]

S = fracture spacing [m]

The resistance in the edge to the plug, R_{R3}

$$R_{R3} = \frac{1}{\pi r_2 D_R \ln(2+\sqrt{5})} \tag{4-9}$$

D_R = the effective diffusivity in the rock [m²/a]
r_2 = the radius of the deposition hole [m]

The resistance in the edge to the fracture, R_{R4}

$$R_{R4} = \frac{1}{\pi r_2 D_R \ln(1+\sqrt{2})} \tag{4-10}$$

The resistance in the rock to the fracture, R_{R6}

$$R_{R6} = \frac{1}{\pi r_2 D_R \ln\left(\frac{\frac{S}{2}-\frac{\delta}{2}+\sqrt{\left(\frac{S}{2}-\frac{\delta}{2}\right)^2+\sigma^2}}{\sigma(1+\sqrt{2})}\right)} \tag{4-11}$$

The resistance in plug, R_{P1} and R_{P2}

$$R_{P1} = \frac{\ln\left(\frac{r_2+\frac{\delta}{2}}{r_2}\right)}{\pi\sigma D_P} \text{ and } R_{P2} = \frac{\ln\left(\frac{r_2+\sigma}{r_2+\frac{\sigma}{2}}\right)}{\pi\sigma D_P} \tag{4-12, 13}$$

Film resistance, R_F

$$R_F = \sqrt{\frac{\Omega}{4\pi D_W u_f (r_2+\sigma)\delta^2}} \tag{4-14}$$

D_W = the diffusivity in free water [m²/a]
$\Omega = \pi/4$, effective contact angle [radian]
$u_f = \frac{S}{\delta}\sqrt{U_{0X}^2 + U_{0Y}^2 + U_{0Z}^2}$ water velocity [m/a]

The resistances R_{C1}, R_{C2}, R_{C6}, R_{R3}, R_{R4}, R_{R6}, R_{P1}, R_{P2} and R_F are added together to form a total resulting resistance for one fracture denoted RRES

according to the equations in Chapter 4 in (Nilson, et al., 1991) and the total resistance RRESCH including R_{CH} and R_{ST} is calculated according to Equation 4-15.

$$R_{RESCH} = R_{CH} + \frac{\frac{R_{ST}R_{RES}}{\mathrm{Int}\left(\frac{H}{S}+1\right)}}{R_{ST} + \frac{R_{RES}}{\mathrm{Int}\left(\frac{H}{S}+1\right)}} \qquad (4\text{-}15)$$

H = depth of deposition hole [m]

$\mathrm{Int}\left(\frac{H}{S}+1\right)$ is the calculation of the number of fractures in the deposition hole.

The function $F\left(a, \beta + \frac{v}{2}\right)$ is defined by:

$$F\left(a, \beta + \frac{v}{2}\right) = \frac{av}{d} + \frac{4d}{\pi}\sum_{n=1}^{\infty} \frac{1}{n^2}\cos^2\left(\frac{\pi n\left(\beta + \frac{v}{2}\right)}{d}\right) \sin\left(\frac{\pi n \frac{v}{2}}{d}\right) \tanh\left(\frac{\pi n \beta}{d}\right) \qquad (4\text{-}16)$$

d = half fracture distance[m]

The convergence of Equation 4-16 is rather slow for very small fracture apertures and the sum is oscillating strongly. To decide if the wanted precision has been obtained, the estimation of the truncation error was based on the expression:

$$\sum_{n=a}^{\infty} \frac{1}{n^2}\cos^2\left(\frac{\pi n\left(\beta + \frac{v}{2}\right)}{d}\right) \sin\left(\frac{\pi n \frac{v}{2}}{d}\right) \tanh\left(\frac{\pi n \beta}{d}\right) < \int_{a}^{\infty} \frac{1}{x^2} dx \qquad (4\text{-}17)$$

That is, if $n = a$ the absolute truncation error is always less than $\frac{4d}{a\pi}$.

4.2 RESULTS FROM TEST RUN WITH RESISTANCE NETWORK MODEL

In order to test the code after the modifications described in Section 4.1 had been done, two test runs were made, one including the resistance caused by the small (R_{CH}) hole in the canister and one assuming that the canister causes no resistance once it is penetrated. The gap inventory was excluded from both these runs. The results are shown in Figures 4-3 and 4-4. The solubilities in salt water was taken from (Bruno and Sellin, 1991).

Table 4-1. Input data used for the calculations

Horizontal Darcy velocity	$1{\cdot}10^{-4}$	($m^3/m^2{\cdot}y$)
Vertical groundwater flowrate	0	($m^3/m^2{\cdot}y$)
Half fissure width i near field	$5{\cdot}10^{-5}$	(m)
Effective diffusivity in clay buffer	$1.6{\cdot}10^{-5}$	(m^2/y)
Diffusivity in flowing water	$6.0{\cdot}10^{-2}$	(m^2/y)
Fissure spacing outside buffer	1.0	(m)
Length of clay plug	0.01	(m)
Distance up to the disturbed zone	2	(m)
Effective diffusivity in rock	$1.6{\cdot}10^{-6}$	(m^2/y)
Effective diffusivity in bentonite plug	$1.6{\cdot}10^{-4}$	(m^2/y)
Inner diameter of canister	0.6	(m)
Outer diameter of canister	0.8	(m)
Diameter of deposition hole	1.5	(m)
Porosity of buffer	0.2	(-)
Density of buffer	2100	(kg/m^3)
Time to canister penetration	100	(years)
Diameter of penetration hole	$2.5{\cdot}10^{-3}$	(m)

There is no difference in the release rates for the nuclides with high solubility but there is a decrease in release rate for the nuclides with a low solubility with more than two orders of magnitude.

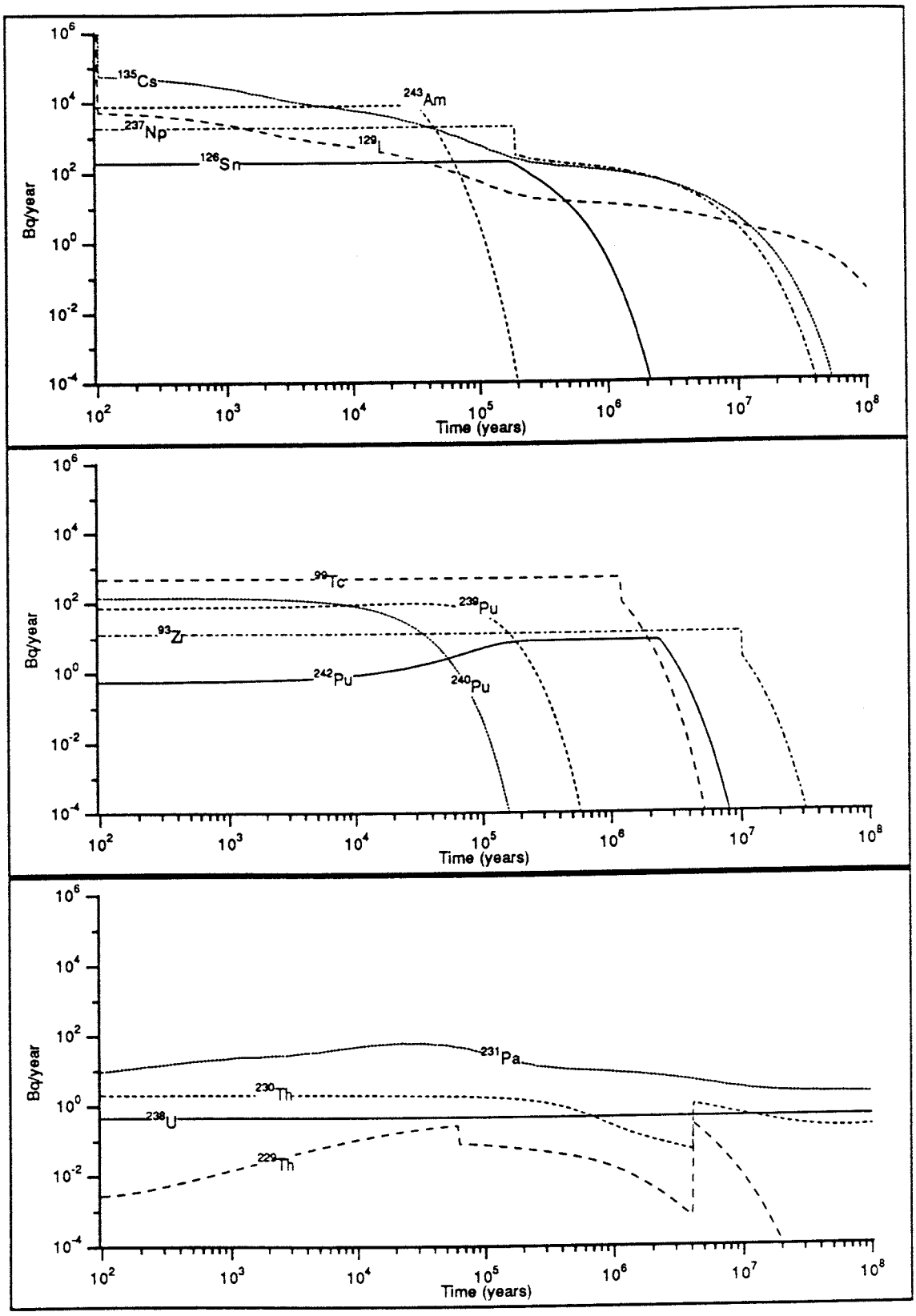

Figure 4-3. Release from the near field of one KBS-3 canister. No resistance from the canister after 100 years.

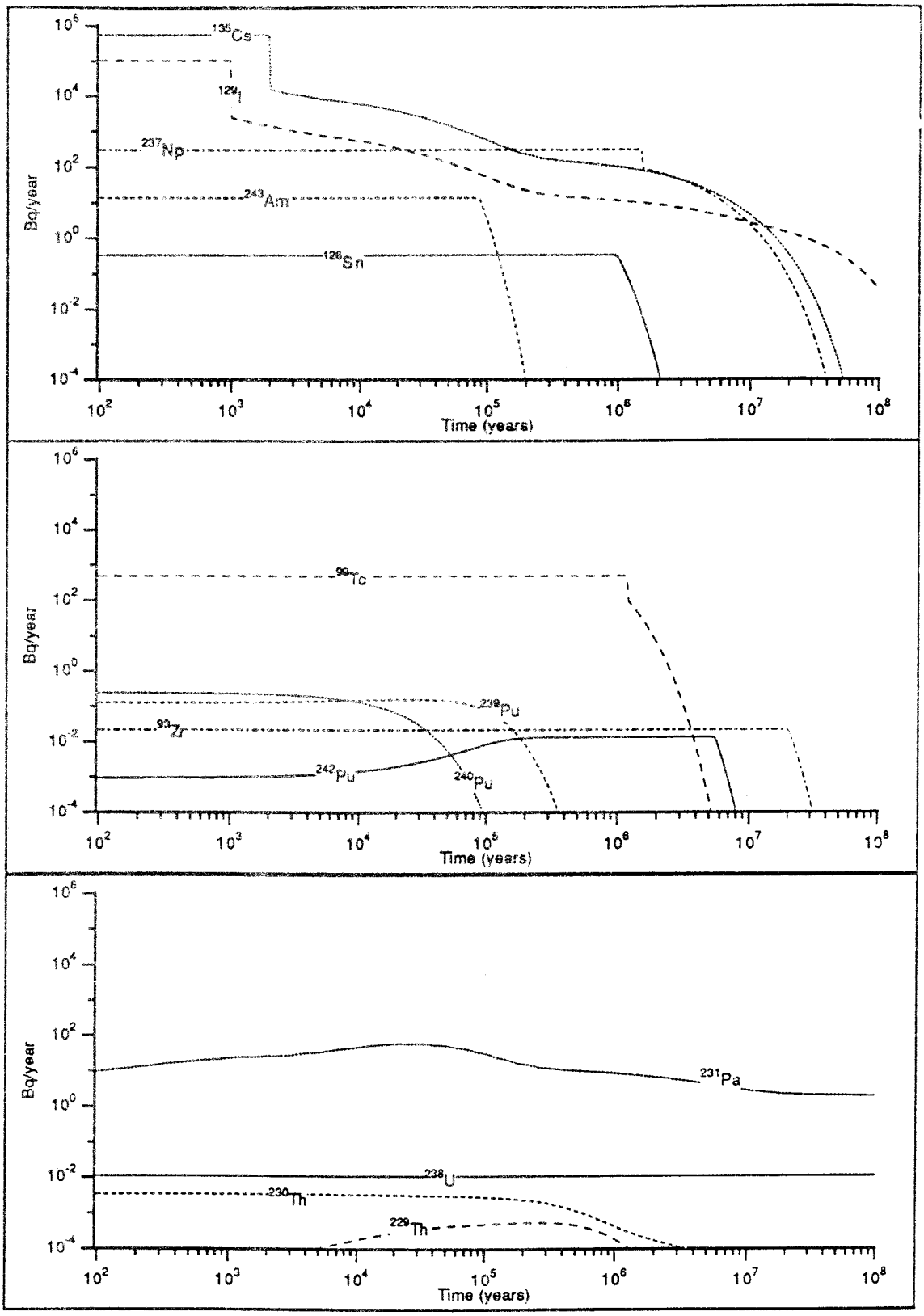

Figure 4-4. Release from the near field of one KBS-3 canister. Canister penetrated by 2.5 mm diameter hole after 100 years.

The results of the test runs with the resistance network model shows that the effect of the limiting the available area at the canister to a hole of small size is of major importance and accordingly the assumption that the hole diameter will remain constant with time will be a crucial parameter for the safety assessment in SKB91. Outside the penetration hole the model predicts that a significant part of the release will be upwards to the disturbed zone. For Cs and I 5 % of the inventory was assumed to be available for instantaneous dissolution which can be seen as an higher release for these two nuclides in the early parts of the curves.

Since the diffusion from a small hole in the canister through the bentonite is so important for the release rates, it would be of interest to make both laboratory and field experiments for comparison with the models for this phenomenon. The characterization of the disturbed zone and experiments for demonstration of the film resistance in the rock are also of interest for future field experiments.

5 CONCLUSIONS

The TULLGARN code is in its the present form available in both standalone and as a PROPER version for use in probabilistic modelling. It can compute the steady state migration rates of radionuclides and decay chains of radionuclides from the near field of KBS-3 canisters. Canister corrosion, diffusive transport, fuel matrix dissolution, solubility limitations at reducing and oxidizing conditions, fast washout of instantly released part of the inventory and chain decay can all be taken into account. The changes made to the code described in Chapter 4 include the resistance caused by the intrusion of bentonite clay into the fractures around the deposition holes and the diffusion paths through the rock into the fractures as well as the path upwards to the disturbed zone. Another important modification of the code was the diffusion resistance caused by the small penetration hole in the canister that for the low solubility nuclides causes a significant decrease of the release rates. For the the handling of the release of the gap inventory several model has been tested but none of them is yet selected to be included in TULLGARN.

6 LITERATURE

Bergström, U. and S. Nordlinder, Individual Radiation Doses from Unit Releases of Long Lived Radionuclides. SKB TR-90-09, 1990.

Bruno, J. and P. Sellin, Radionuclide solubilities to be used in SKB 91, Version I. SKB AR 91-02, 1991.

Carslaw H.S. and J.C. Jaeger
Conduction of Heat in Solids, 2nd. ed.,
Oxford Univ. Press, New York, 1959

Nilson, L., L. Moreno, I. Neretnieks and L. Romero, A Resistance Network Model Describing the Transport of Radionuclides into the Near Field Surrounding a Repository for Nuclear Waste. SKB TR In preparation, 1991.

Norman, S. and Kjellbert, NEAR21 — A Near Field Radionuclide Migration Code for use with the PROPER Package. SKB TR In preparation, 1991.

Widén, H., J. Bjelkås and B. Grundfelt, Preliminary Near-field Calculations for SKB91. Kemakta Consultants AB, Stockholm, Sweden Working report, SKB AR 90-35, 1990.

7 NOTATION

A	Area	[m^2]
A_{Dep}	the area of the deposition hole	[m^2]
a	bentonite thickness	[m]
a	Inner radius of hollow sphere or cylinder	[m]
b	Outer radius of hollow sphere or cylinder	[m]
C_0	Concentration at boundary	[mol/m^3]
D_e	Effective diffusivity (Defined by $D_p\varepsilon_p$)	[m^2/a]
D_C	he effective diffusivity in the clay	[m^2/a]
D_p	Pore diffusivity	[m^2/a]
D_R	he effective diffusivity in the rock	[m^2/a]
D_W	the diffusivity in free water	[m^2/a]
d	half fracture distance	[m]
d_h	the diameter of the deposition hole	[m]
$F\left(a, \beta + \frac{\gamma}{2}\right)$	is defined in Equation 4-16.	
H	depth of deposition hole	[m]
K_d	Mass sorption coefficient	[m^3/kg]
L_{ST}	distance from the penetration hole up to the disturbed zone	[m]
l	Length	[m]
Q	Release rate	[mol/a]
q_{eq}	Equivalent water flow rate	[m^3/a]
r	radius	[m]
r_2	the radius of the deposition hole	[m]
S	fracture spacing	[m]
u_f	water velocity	[m/a]

Greek letters

α	Mass transfer coefficient	[m^2/a]
β	parameter in Equation 4-16	[m]
ε_p	Porosity	[m^3/m^3]
θ	Centre angle of wedge.	[radians]
ϕ	Solid angle of a cone	[steradians]
λ	the diameter of the penetration hole	[m]
ν	parameter in Equation 4-16	[m]
ρ	Density	[kg/m^3]
$\Omega = \pi/4$	effective contact angle	[radian]

APPENDIX 1

RESULT PLOTS FOR THE GLACIATION SCENARIOS, ONE CANISTER

These diagrams show the release from the near field calculated with NEAR21 with the α-radiolysis model, Figures A1-1 to A1-6. All the plots in this appendix are for calculations on only one canister. The calculations were made with identical data except for the time when the copper canister is penetration according to Table A1-1.

Table A1-1. Definition of base cases, 1 to 6.

Case #	penetration time [years]	reason for canister failure
1	100	construction error
2	25000	glaciation
3	65000	glaciation
4	125000	glaciation
5	10^6	inner over pressure
6	corrosion dependent	corrosion

APPENDIX 1

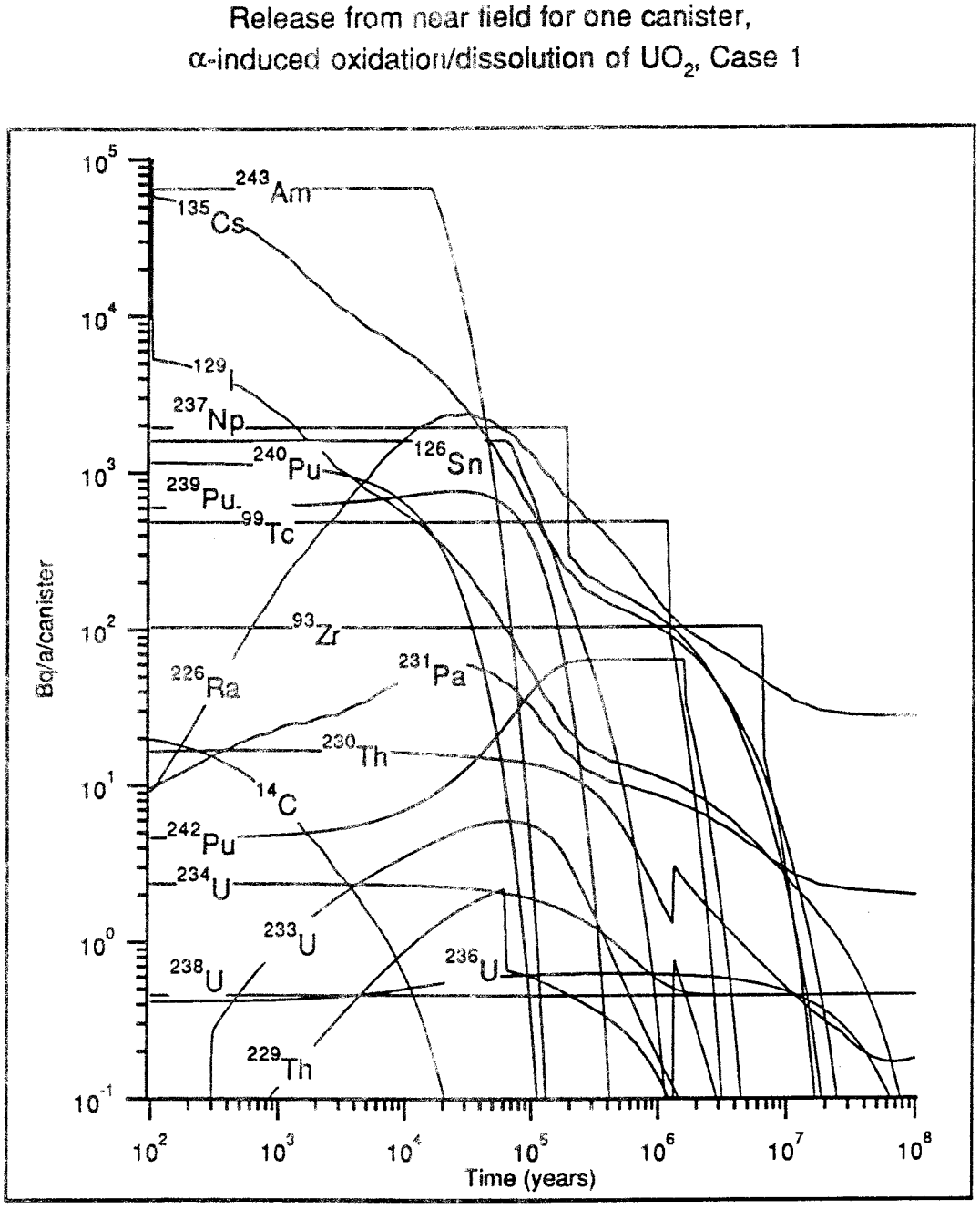

Figure A1-1. Results from Case 1, α-radiolysis model.

APPENDIX 1

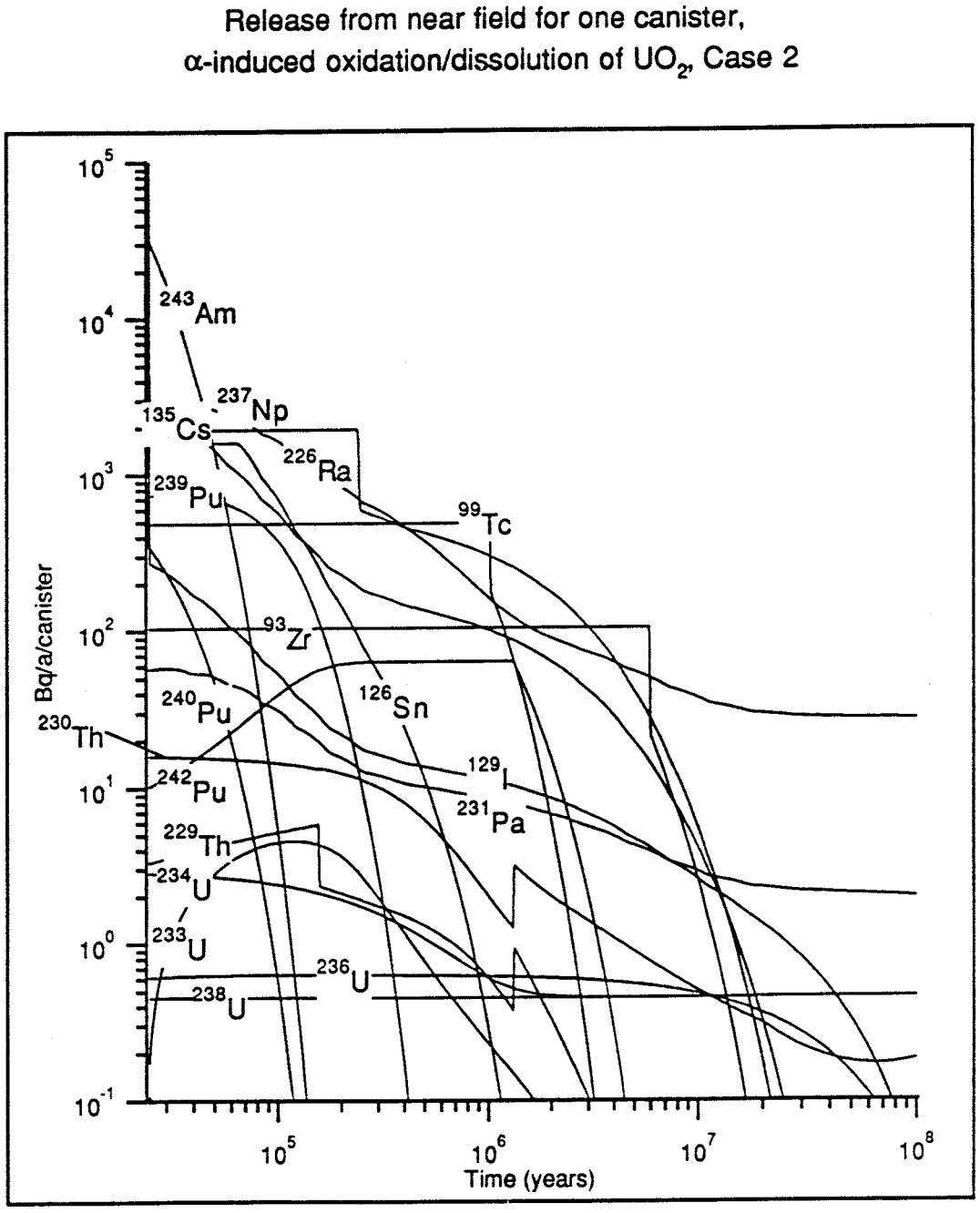

Figure A1-2. Results from Case 2, α-radiolysis model.

APPENDIX 1

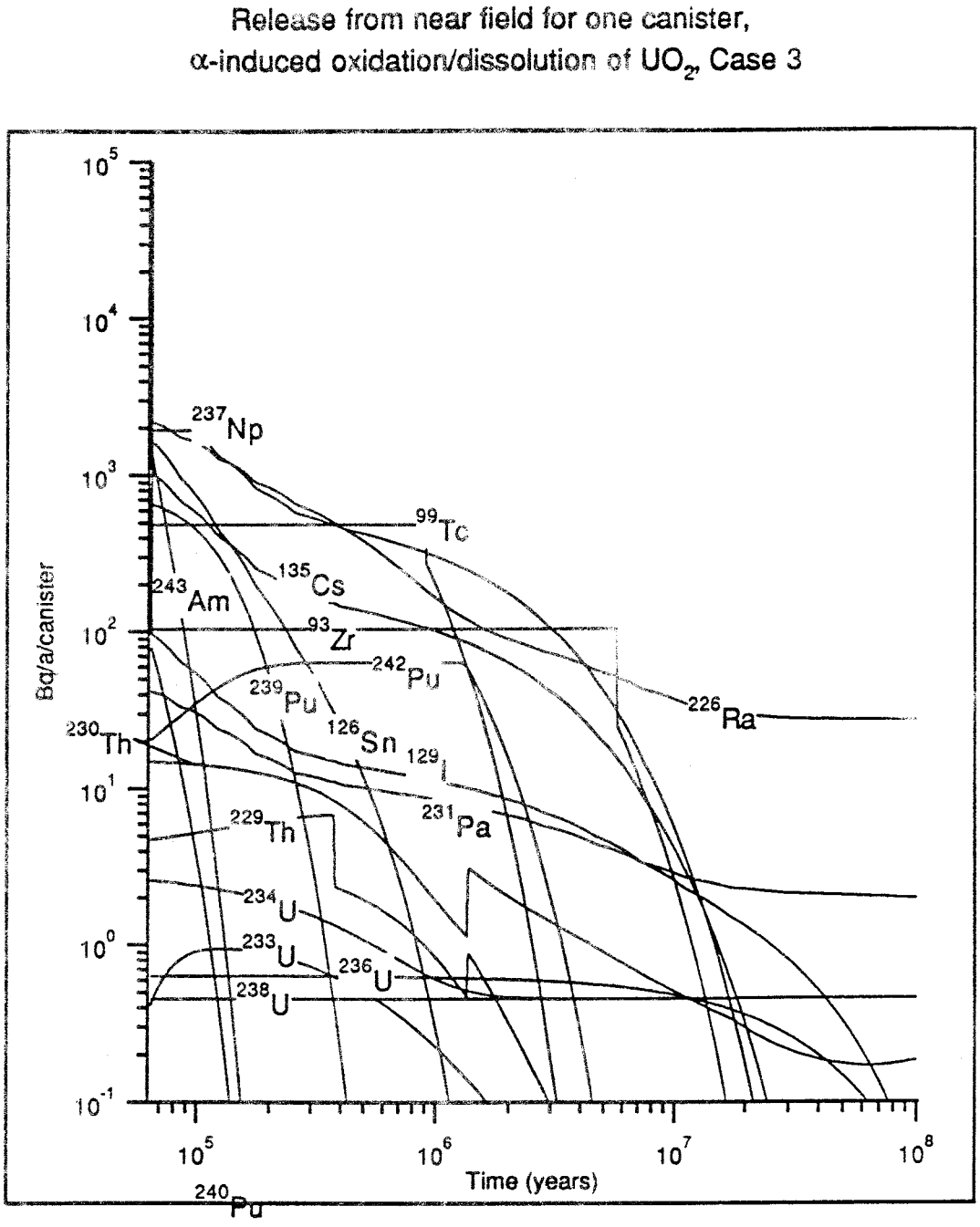

Figure A1-3. Results from Case 3, α-radiolysis model.

APPENDIX 1

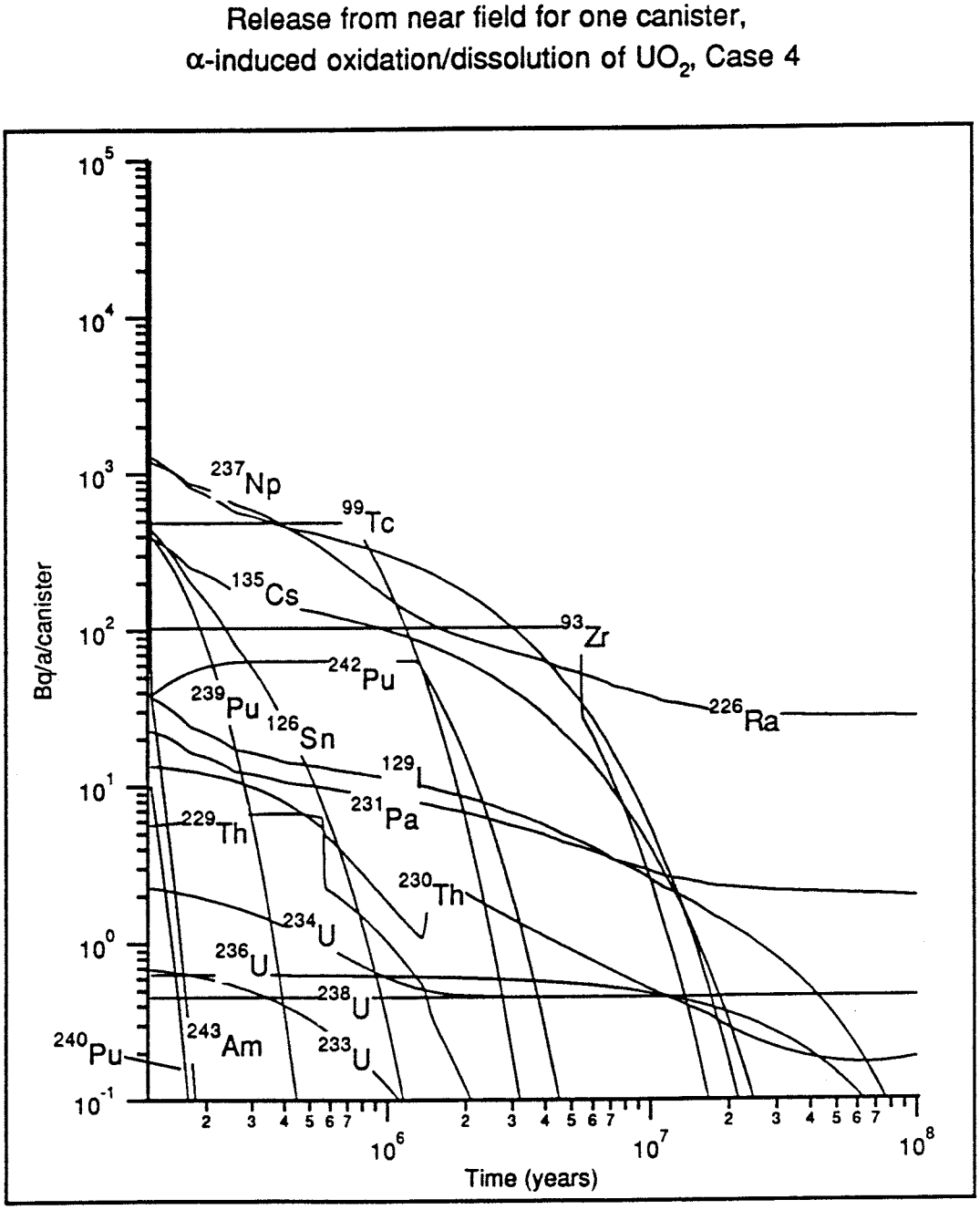

Figure A1-4. Results from Case 4, α-radiolysis model.

APPENDIX 1

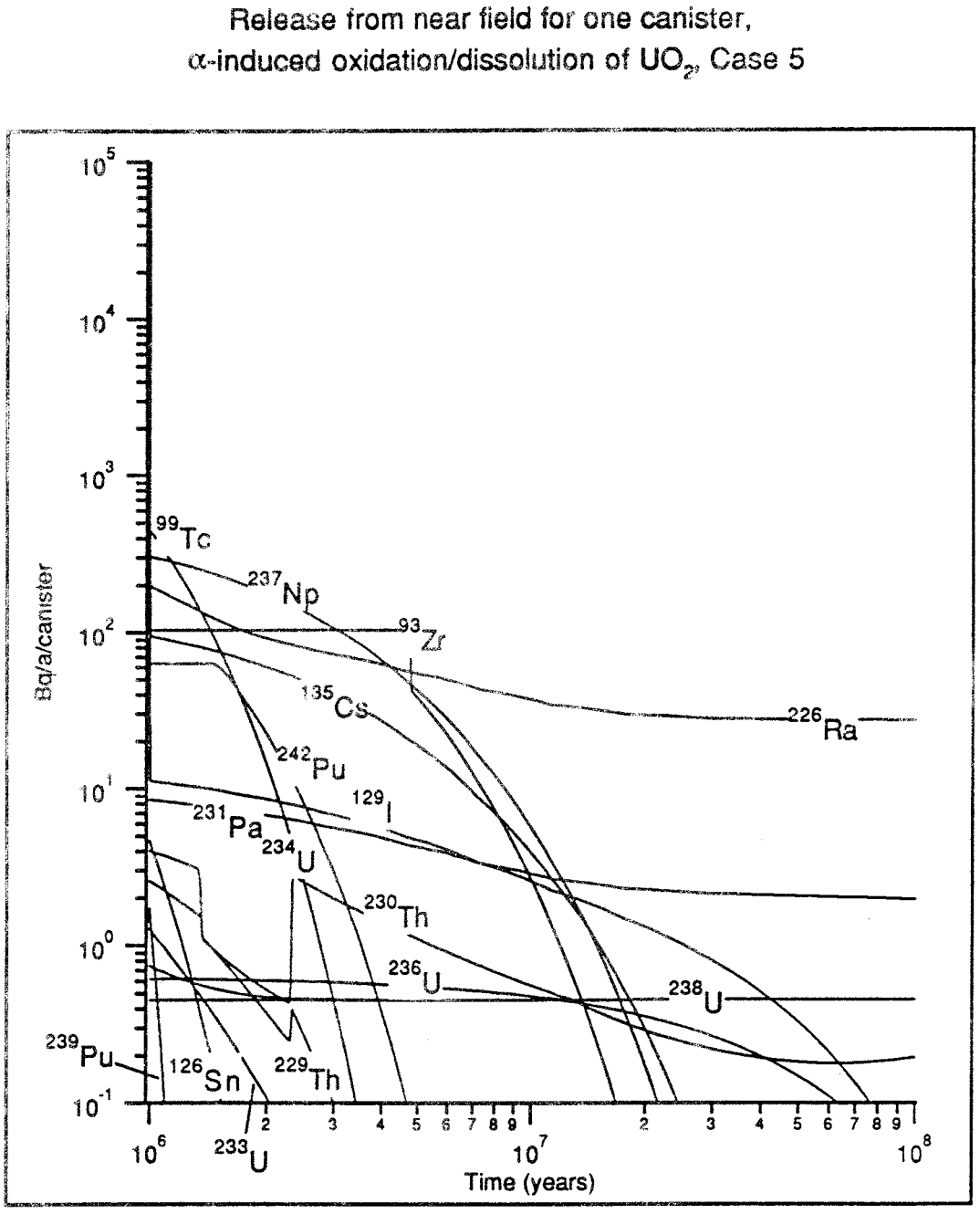

Figure A1-5. Results from Case 5, α-radiolysis model.

APPENDIX 1

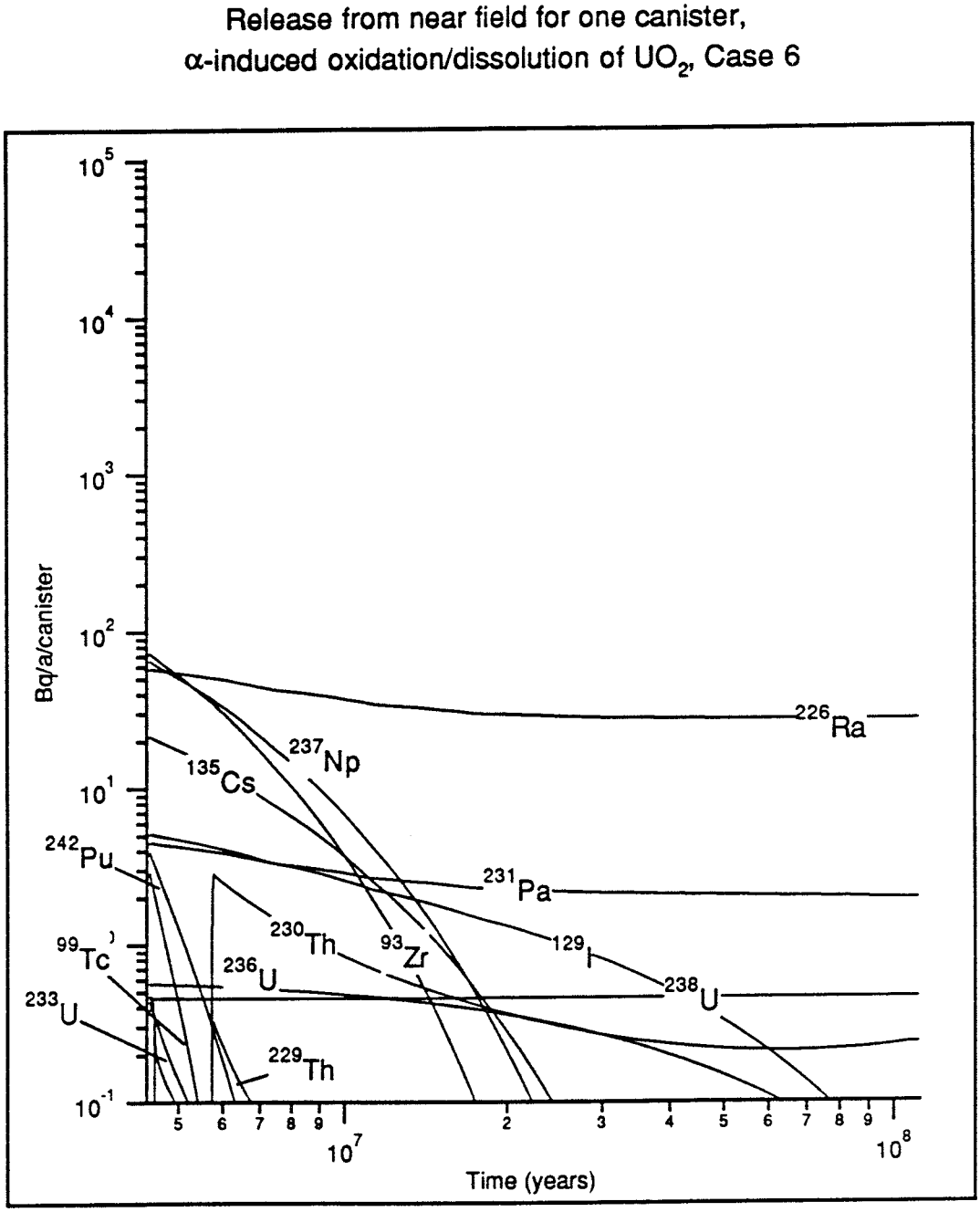

Figure A1-6. Results from Case 6 α-radiolysis model.

APPENDIX 2

RESULT PLOTS FOR THE GLACIATION SCENARIOS, 5300 CANISTERS

The diagrams below show the release from the near field calculated with NEAR21 with the α-radiolysis model. Table A2-1 defines how the combination cases are built from the base cases 1 to 6 that are defined in Table A1-1

Table A2-1. Definition of combination cases give as % of canisters penetrated according to respective base case. For cases O and P the actual number of canisters are give instead of percent of all canisters.

case	1	2	3	4	5	6
J	1	10	20	30	0	39
K	1	10	10	10	0	69
L	1	30	20	10	0	39
M	10	10	10	10	0	60
N	1	10	10	10	69	0
O	1	0	0	0	5299	0
P	1	0	0	0	0	5299
Q	1	0	0	0	99	0
R	1	0	0	0	0	99

APPENDIX 2

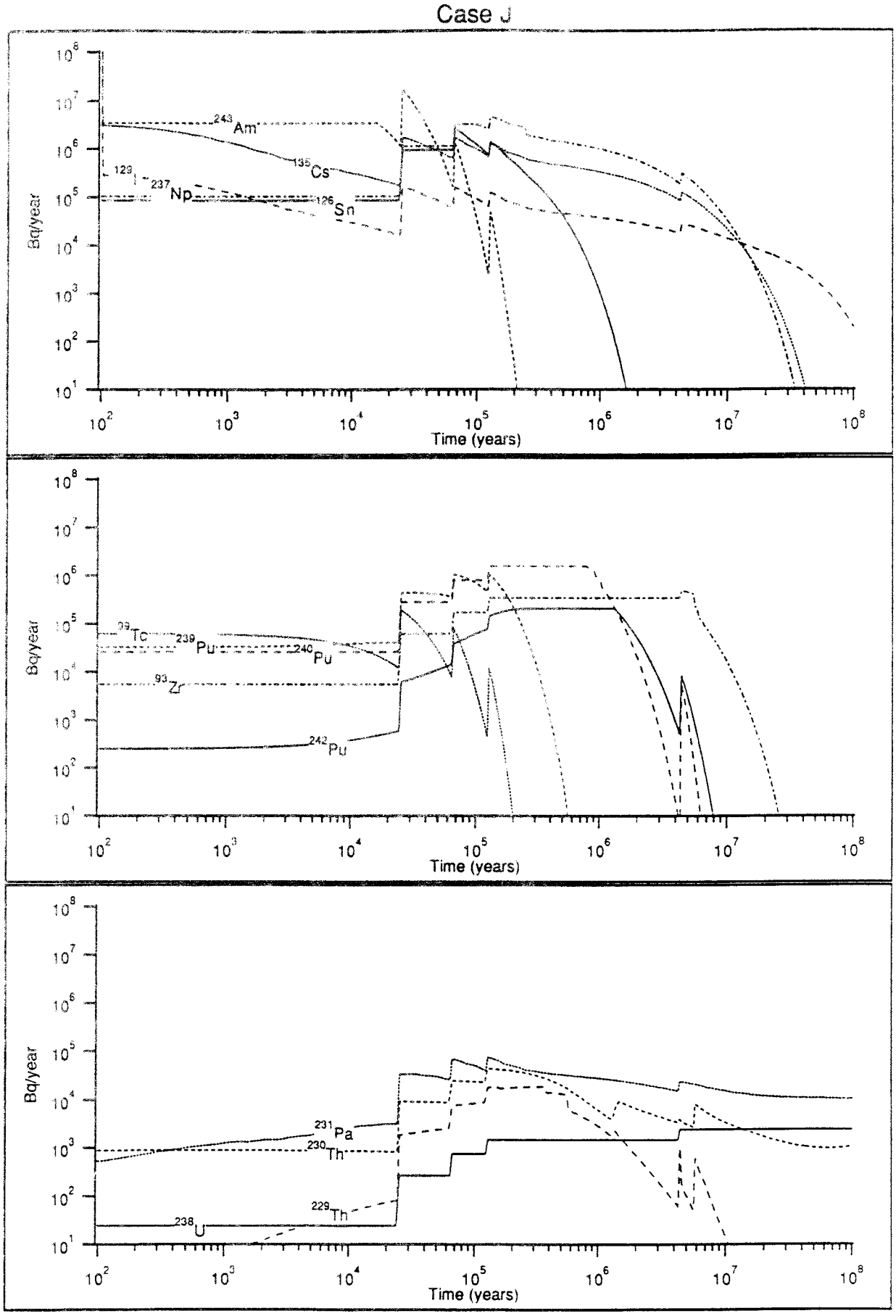

Figure A2-1. Results from Case J, α-radiolysis model, Bq/year.

APPENDIX 2

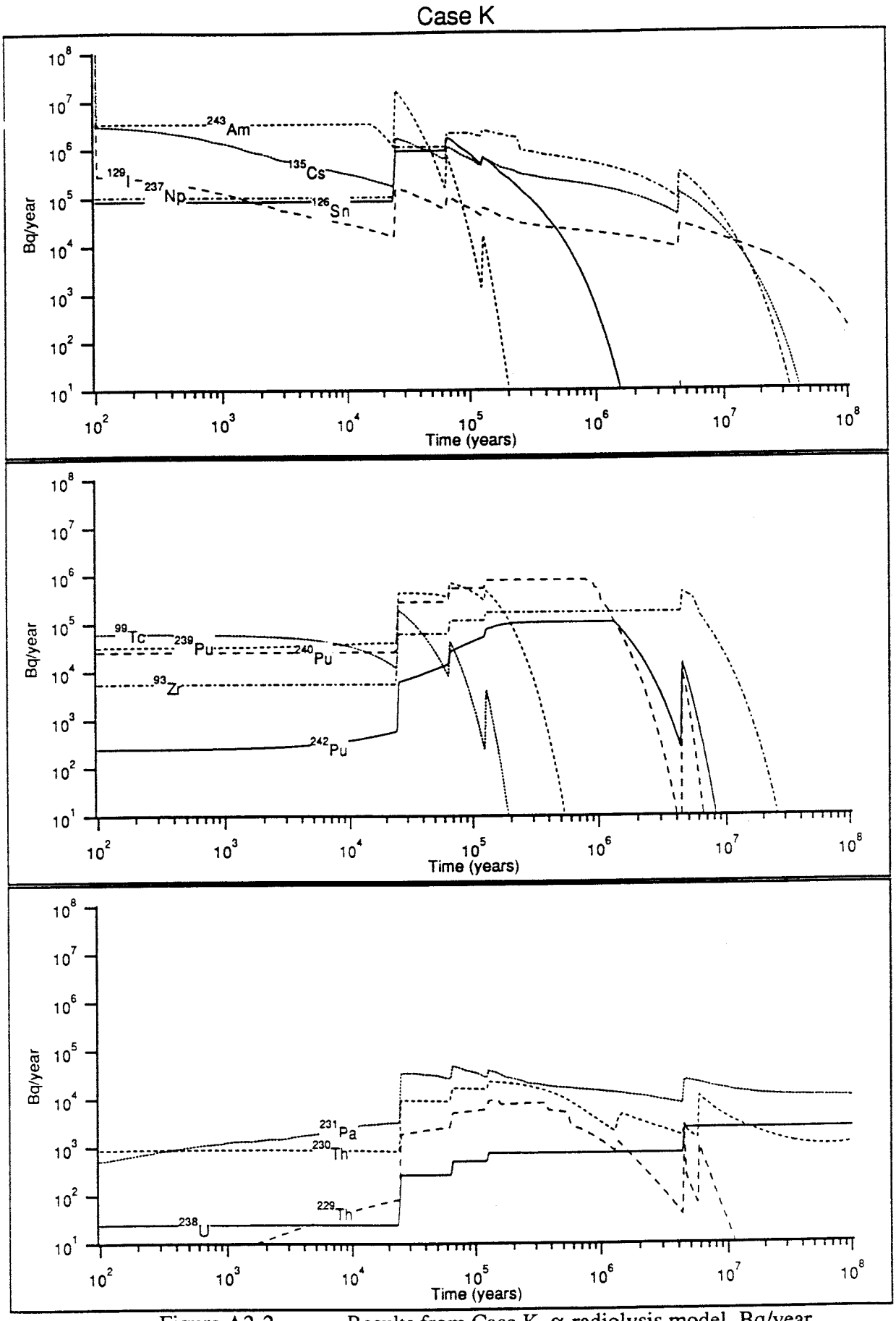

Figure A2-2. Results from Case K, α-radiolysis model, Bq/year.

APPENDIX 2

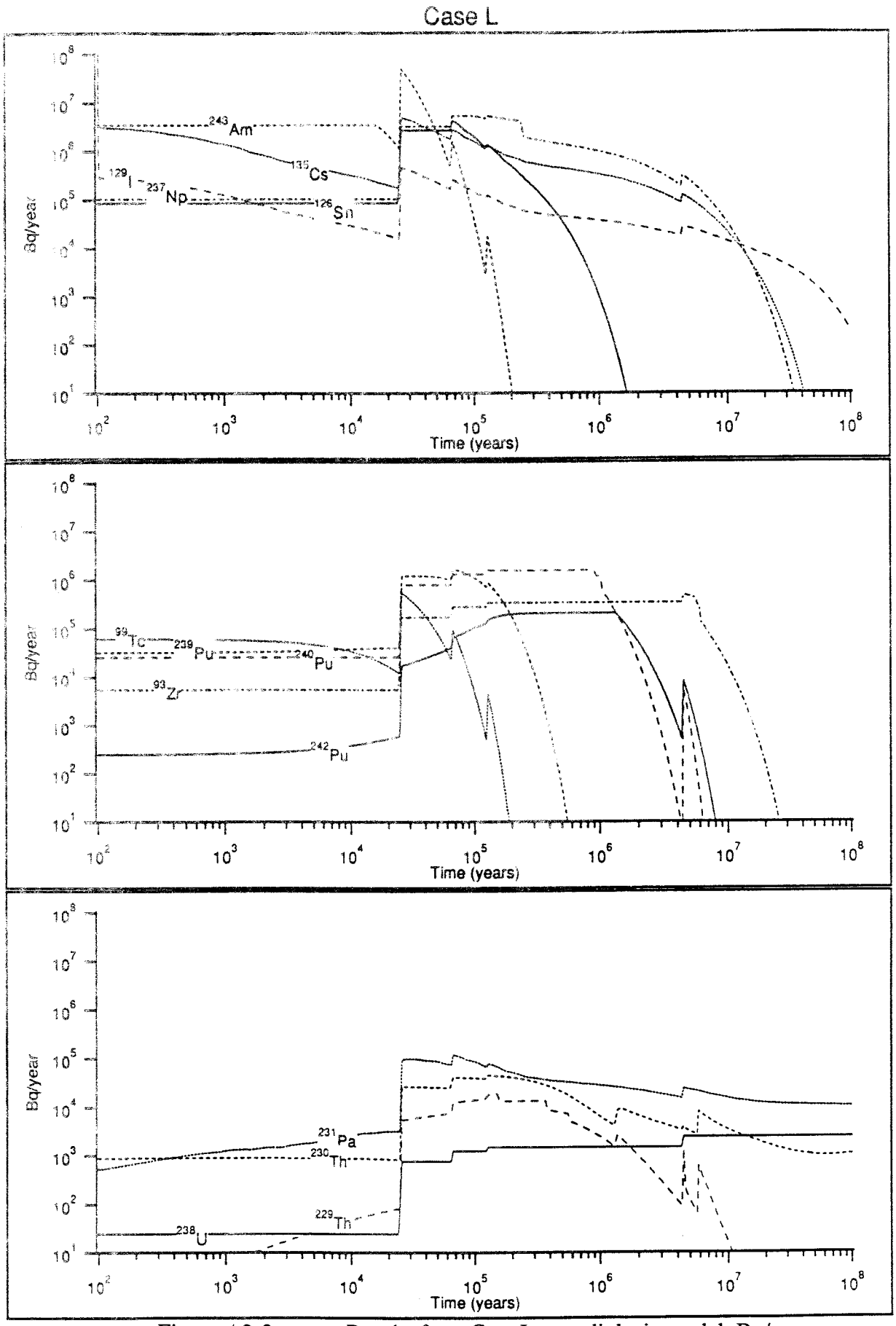

Figure A2-3. Results from Case L, α-radiolysis model, Bq/year.

APPENDIX 2

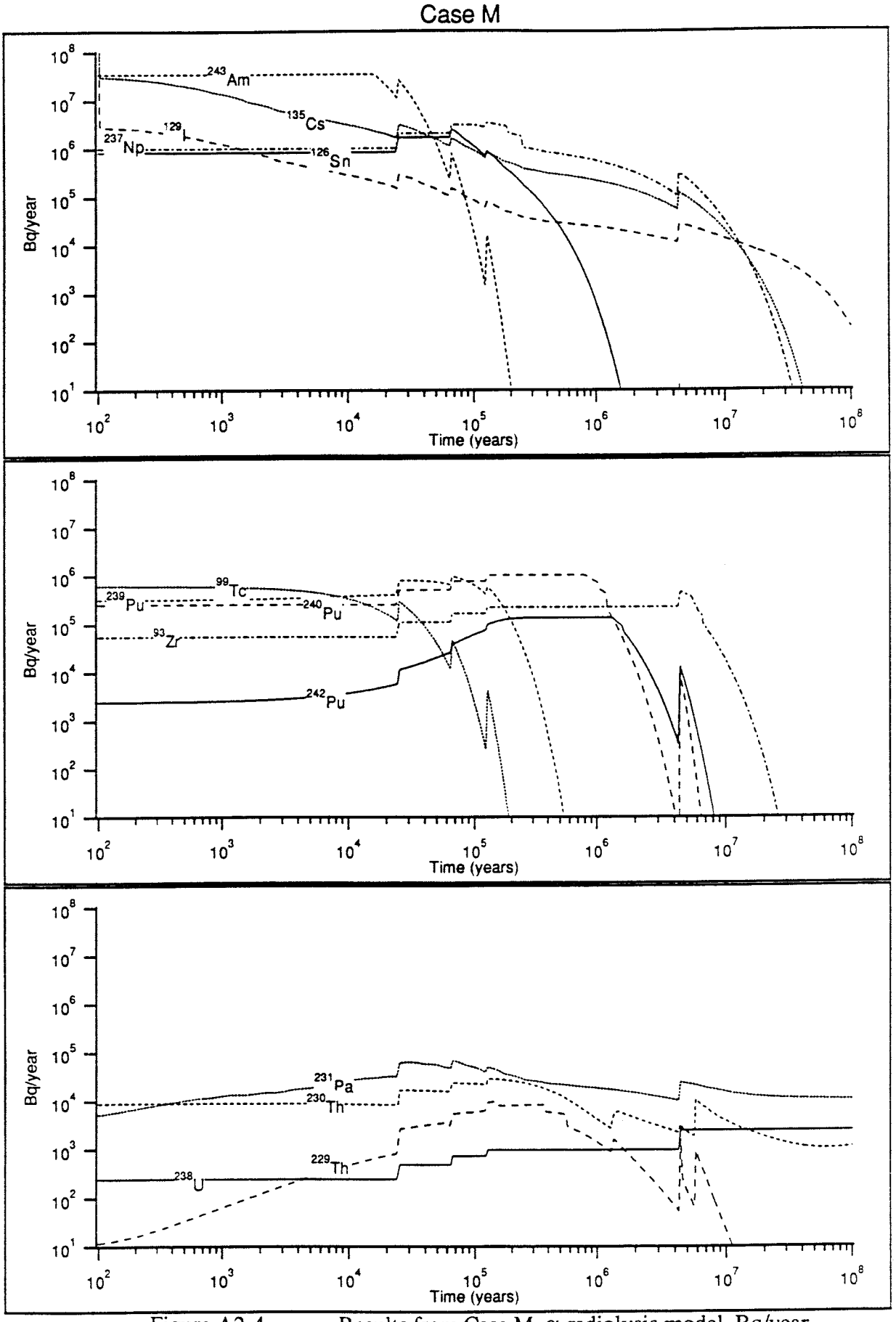

Figure A2-4. Results from Case M, α-radiolysis model, Bq/year.

APPENDIX 2

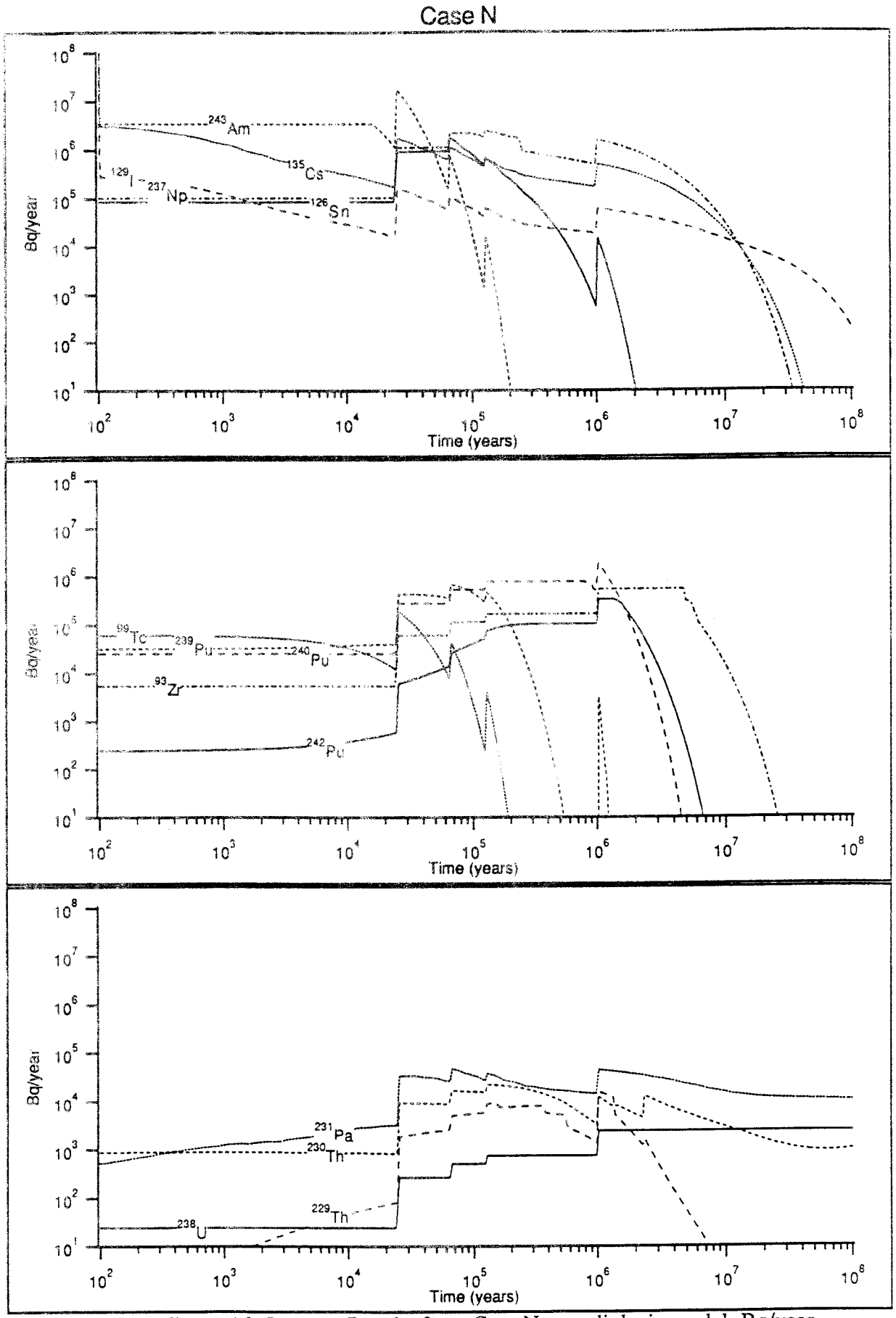

Figure A2-5. Results from Case N, α-radiolysis model, Bq/year.

APPENDIX 2

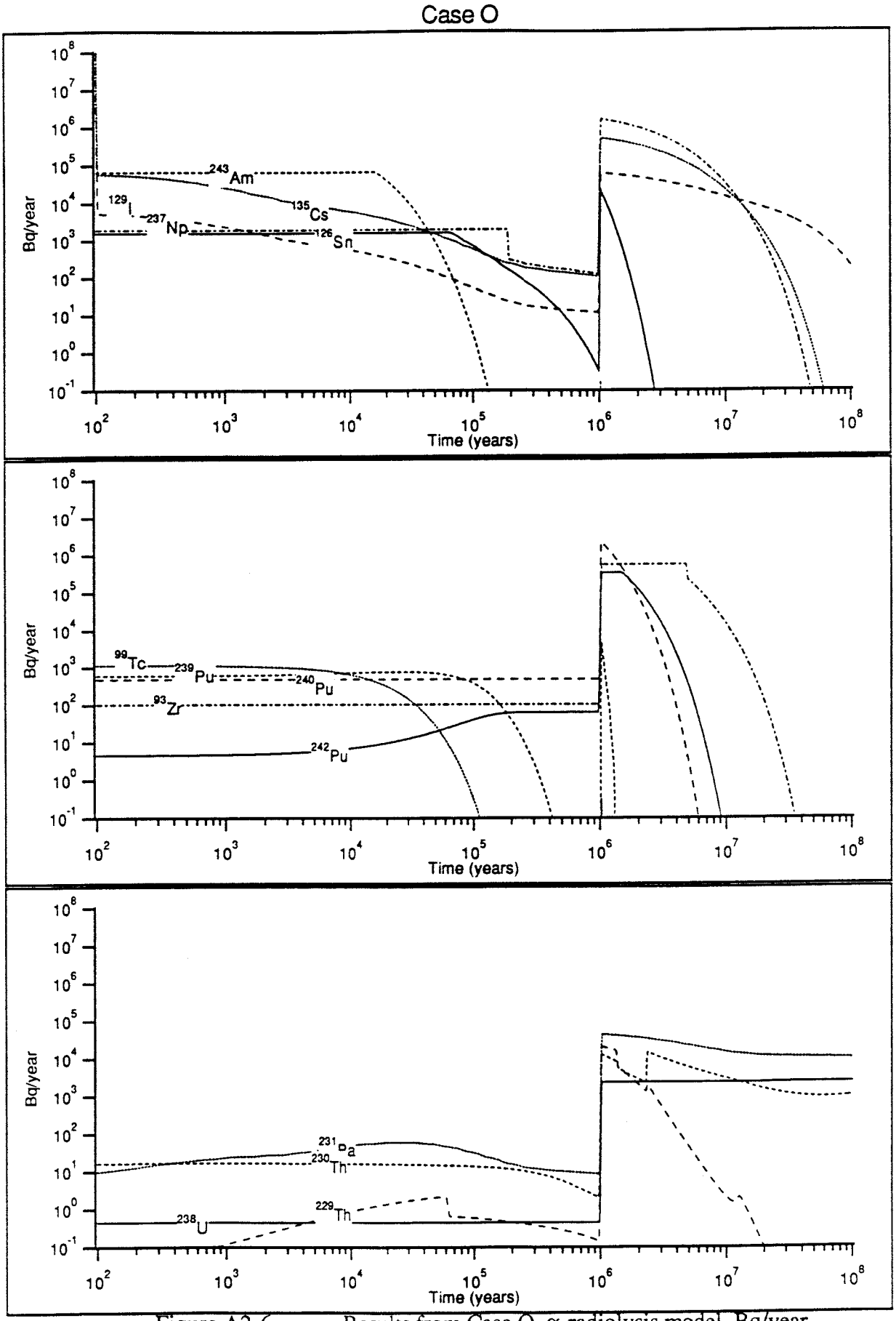

Figure A2-6. Results from Case O, α-radiolysis model, Bq/year.

APPENDIX 2

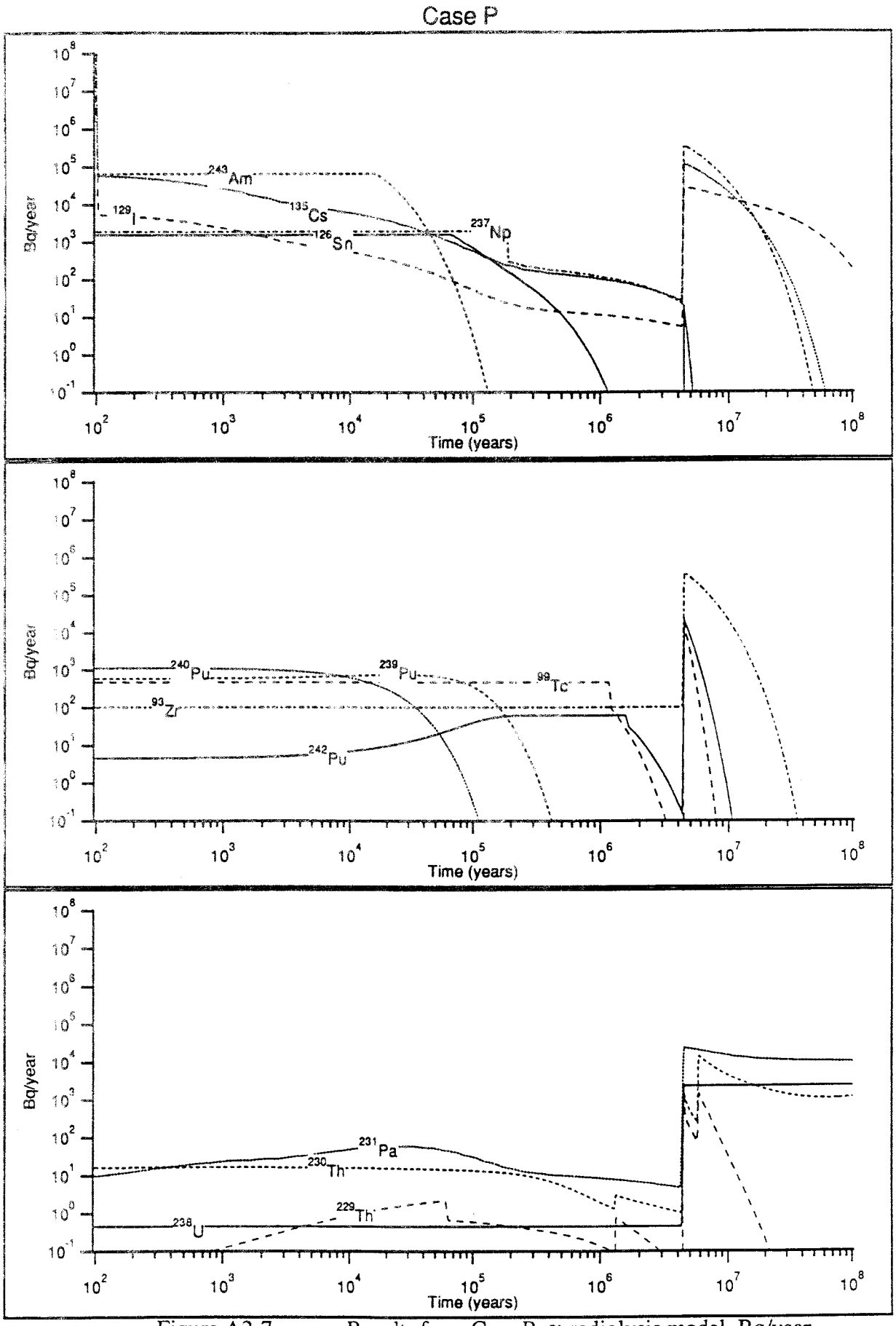

Figure A2-7. Results from Case P, α-radiolysis model, Bq/year.

APPENDIX 2

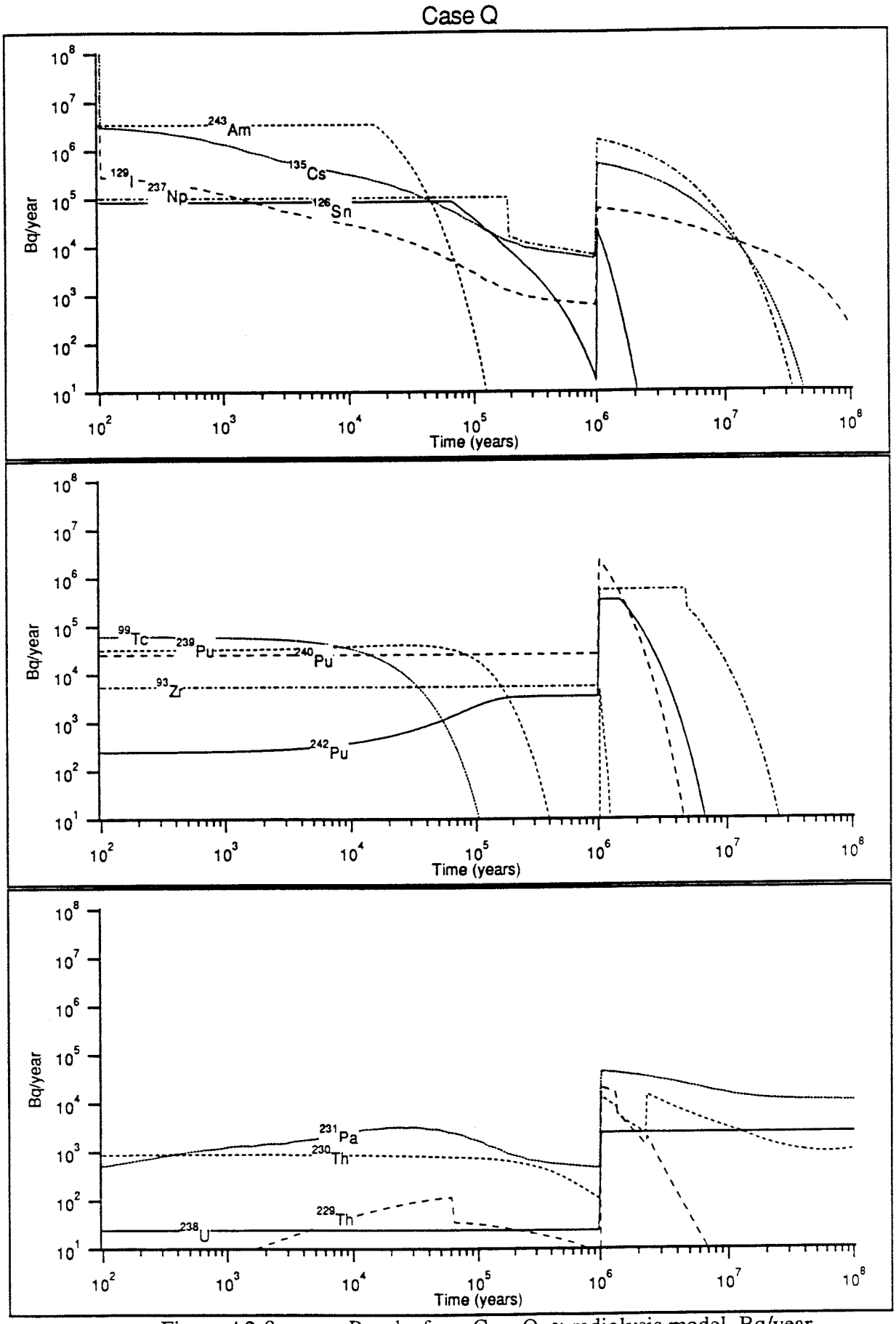

Figure A2-8. Results from Case Q, α-radiolysis model, Bq/year.

APPENDIX 2

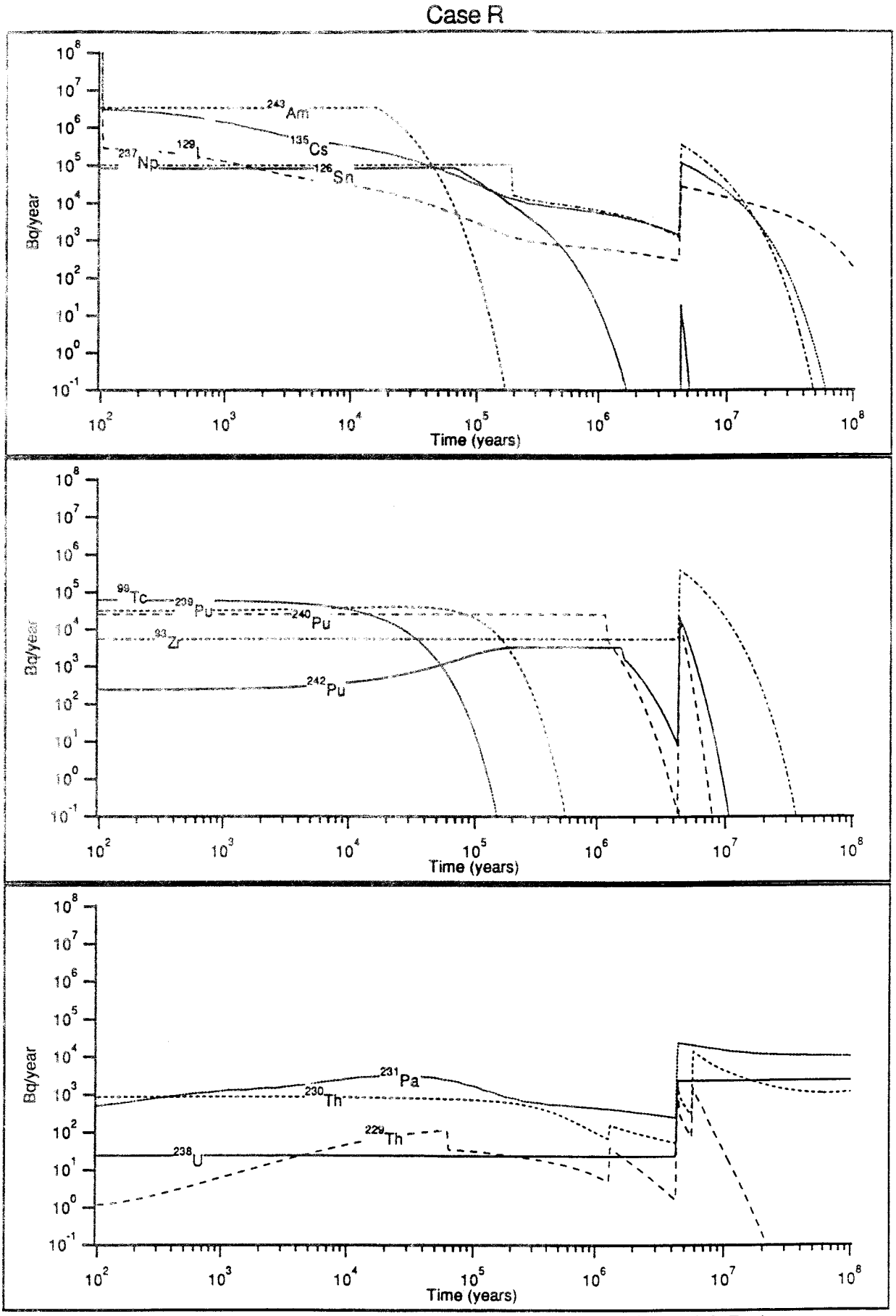

Figure A2-9. Results from Case R, α-radiolysis model, Bq/year.

APPENDIX 3

COMPARISON OF TWO METHODS FOR CALCULATION THE RELEASE OF THE READILY DISSOLVABLE SPECIES FROM A KBS-3 CANISTER

ABSTRACT

The release rate of the soluble cesium and iodine that is accumulated in the fuel-cladding gaps and grain boundaries was studied in this project. An analytic solution was used that assumes instantaneous dissolution of the soluble species and that the mass transfer resistance is controlled by molecular diffusion. The model is based on a porous media for both the bentonite buffer and the rock outside the buffer. Runs were also made to make a comparison with a code that uses numerical solution to solve the same problem but in cylindrical coordinates and without the resistance from the rock outside the buffer. The calculated release rates and the CPU-times required by the two programs were compared. As expected, the analytic model gave lower release rates due to the resistance caused by the rock. The numerical model used about 20 times more CPU-time. It was found that both models are useful for estimating the release rates of the readily dissolvable species in HLW.

APPENDIX 3

INTRODUCTION

Among the most important factors for the safety of a KBS-3 type of repository are the release rates of the soluble species ^{129}I, ^{135}Cs and ^{137}Cs. This report concerns a study of two models for this type of calculations. One analytical model that has been developed at University of California called UCBNE108, and one numerical solution developed at SKB, called PULSE. The aim is to find a model that can be incorporated into the NEAR21 code (TULLGARN) which at present only can handle nuclides that are inside the fuel matrix. The readily dissolvable part of ^{129}I, ^{135}Cs and ^{137}Cs are released as a very short pulse.

APPENDIX 3

DESCRIPTION OF THE MODEL

The NEAR21 code (Norman and Kjellbert, 1990) that is used for the calculations of the release of radionuclides from the near field of KBS-3 canisters cannot handle the instationary part of the diffusion process. To model this, for the readily dissolvable species, ^{129}I, ^{135}Cs and ^{137}Cs, is important because these nuclides, in particular ^{129}I, can be expected to be among the dominating.

An analytic model for mass transfer of soluble species into backfill and porous rock has been described (Kang and Lee, 1989). The modelled situation is shown in Figure A3-1.

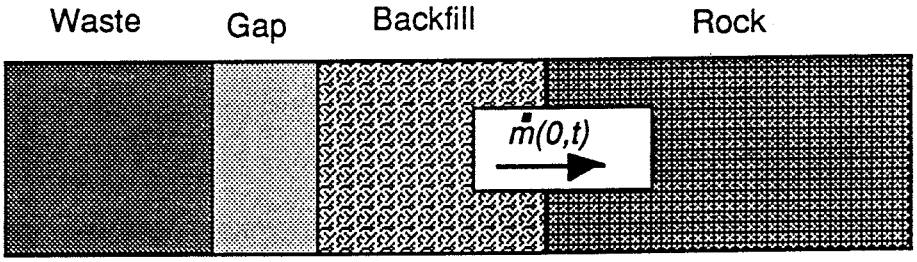

Figure A3-1. Release of soluble species into backfill and rock.

A users manual of this model called UCBNE108 is included last in this Appendix.

The othe code called PULSE is based on a numeric inversion of the Laplace-transformed diffusion equation for cylindrical geometry assuming a zero-concentration boundary condition outside the bentonite buffer.

PERFORMED CALCULATIONS

Calculations were performed for the three nuclides mentioned above with both codes. The input data considering the diffusivities are handled a bit different by the to codes but data were selected so that the apparent diffusivities in the bentonite should be equal. In Table A3-1 and A3-2 the input data used for PULSE is compiled.

APPENDIX 3

Table A3-1. Data used in the calculations with PULSE.

Diameter of canister	0.8	[m]
Diameter of deposition hole	1.5	[m]
Density of dry bentonite	1800	[kg/m^3]
porosity of buffer	0.2	[-]
Inventory of nuclide	1	[mol]
% in gap	100%	[-]

Table A3-2. Nuclide specific data used in the calculations with PULSE.

Data for ^{129}I:		
Half-life	$1.7 \cdot 10^7$	[years]
effective diffusivity	$2.1 \cdot 10^{-12}$	[m^2/s]
K_d-value	0	[m^3/kg]
Data for ^{135}Cs:		
Half-life	$3 \cdot 10^6$	[years]
effective diffusivity	$3 \cdot 10^{-9}$	[m^2/s]
K_d-value	1.4	[m^3/kg]
Data for ^{137}Cs:		
Half-life	30.	[years]
effective diffusivity	$3 \cdot 10^{-9}$	[m^2/s]
K_d-value	1.4	[m^3/kg]

The input data for UCBNE108 was chosen to make the transport conditions in the bentonite equal to the input used for PULSE but with an added resistance caused by the the rock outside the buffer. The apparent diffusivity in the rock was set to a value ten times lower than in the bentonite for all three species.

APPENDIX 3

RESULTS

Only one test run for each of the three nuclides was performed according to the input data specified in Tables A3-1 and A3-2. The relative release rates were plotted in the same diagram with the output from UCBNE108 marked with dashed curves.

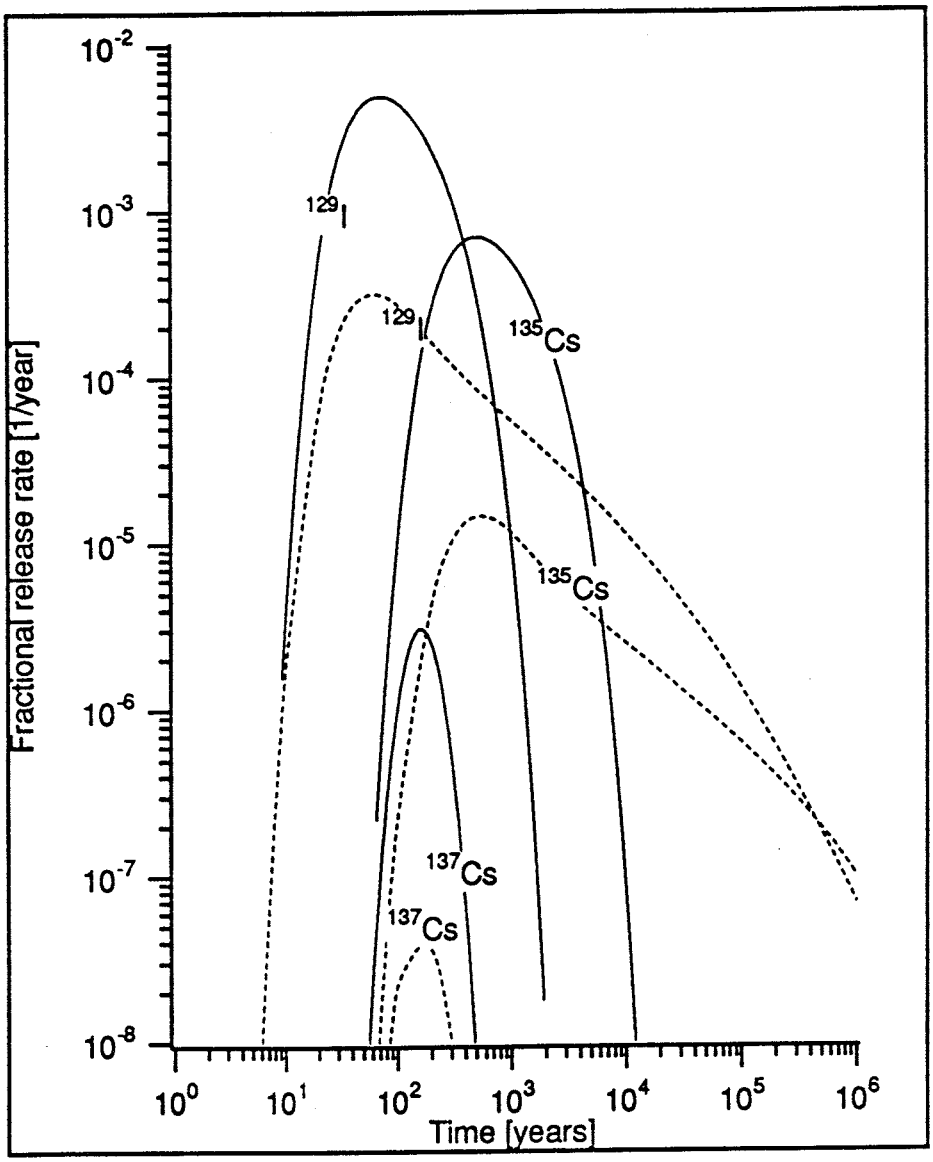

Figure A3-2. Fractional release rate of the soluble species ^{129}I, ^{135}Cs and ^{137}Cs through 35 cm of bentonite backfill, the solid curves were calculated with PULSE and the dashed curves with UCBNE108.

APPENDIX 3

CONCLUSIONS

- Both models release 100 % of the inventory if the inventory consists of a stable species.

- The analytic model give a longer "tail" on the release curves because of the concentration buildup in the rock outside the buffer.

- The time to maximum release rates are similar when the apparent diffusivities are equal but with a lower peak for UCBNE108.

- UCBNE108 is more than 20 times faster on the SKB C210 computer than PULSE which requires about 2.5 seconds of CPU-time for each nuclide.

- Either model could be incorporated into NEAR21, but the execution times for PULSE might be a big disadvantage for the use in probabilistic modelling.

- UCBNE108 is straightforward to include in NEAR21. As we are less familiar with the PULSE code, we cannot estimate the amount of work that would be needed to implement it into NEAR21.

- Use of a compartment model instead may make it possible to calculate the transient release of all nuclides without making the computer execution times to long.

- We recommend that these programs are complemented by TRUMP-calculations that can handle different geometries, for example diffusion from a small hole in a canister and diffusion to a fracture opening as has been investigated in Chapter XX in this Report.

APPENDIX 3

LITERATURE

Norman, S. and N. Kjellbert, NEAR21 — A Near Field Radionuclide Migration Code for use with the PROPER Package.SKB TR in preparation.

Kang, C. L. and W. W.-L. Lee, UCB-NE-108 Users manual, LBL-27044, UCB-NE-4143, 1989.

List of SKB reports

Annual Reports

1977-78
TR 121
KBS Technical Reports 1 – 120
Summaries
Stockholm, May 1979

1979
TR 79-28
The KBS Annual Report 1979
KBS Technical Reports 79-01 – 79-27
Summaries
Stockholm, March 1980

1980
TR 80-26
The KBS Annual Report 1980
KBS Technical Reports 80-01 – 80-25
Summaries
Stockholm, March 1981

1981
TR 81-17
The KBS Annual Report 1981
KBS Technical Reports 81-01 – 81-16
Summaries
Stockholm, April 1982

1982
TR 82-28
The KBS Annual Report 1982
KBS Technical Reports 82-01 – 82-27
Summaries
Stockholm, July 1983

1983
TR 83-77
The KBS Annual Report 1983
KBS Technical Reports 83-01 – 83-76
Summaries
Stockholm, June 1984

1984
TR 85-01
Annual Research and Development Report 1984
Including Summaries of Technical Reports Issued during 1984. (Technical Reports 84-01 – 84-19)
Stockholm, June 1985

1985
TR 85-20
Annual Research and Development Report 1985
Including Summaries of Technical Reports Issued during 1985. (Technical Reports 85-01 – 85-19)
Stockholm, May 1986

1986
TR 86-31
SKB Annual Report 1986
Including Summaries of Technical Reports Issued during 1986
Stockholm, May 1987

1987
TR 87-33
SKB Annual Report 1987
Including Summaries of Technical Reports Issued during 1987
Stockholm, May 1988

1988
TR 88-32
SKB Annual Report 1988
Including Summaries of Technical Reports Issued during 1988
Stockholm, May 1989

1989
TR 89-40
SKB Annual Report 1989
Including Summaries of Technical Reports Issued during 1989
Stockholm, May 1990

Technical Reports

List of SKB Technical Reports 1991

TR 91-01
Description of geological data in SKB's database GEOTAB
Version 2
Stefan Sehlstedt, Tomas Stark
SGAB, Luleå
January 1991

TR 91-02
Description of geophysical data in SKB database GEOTAB
Version 2
Stefan Sehlstedt
SGAB, Luleå
January 1991

TR 91-03
1. The application of PIE techniques to the study of the corrosion of spent oxide fuel in deep-rock ground waters
2. Spent fuel degradation
R S Forsyth
Studsvik Nuclear
January 1991

TR 91-04
Plutonium solubilities
I Puigdomènech[1], J Bruno[2]
[1]Enviromental Services, Studsvik Nuclear, Nyköping, Sweden
[2]MBT Tecnologia Ambiental, CENT, Cerdanyola, Spain
February 1991

TR 91-05
Description of tracer data in the SKB database GEOTAB
SGAB, Luleå
April, 1991

TR 91-06
Description of background data in the SKB database GEOTAB
Version 2
Ebbe Eriksson, Stefan Sehlstedt
SGAB, Luleå
March 1991

TR 91-07
Description of hydrogeological data in the SKB's database GEOTAB
Version 2
Margareta Gerlach[1], Bengt Gentzschein[2]
[1]SGAB, Luleå
[2]SGAB, Uppsala
April 1991

TR 91-08
Overview of geologic and geohydrologic conditions at the Finnsjön site and its surroundings
Kaj Ahlbom[1], Sven Tirén[2]
[1]Conterra AB
[2]Sveriges Geologiska AB
January 1991

TR 91-09
Long term sampling and measuring program. Joint report for 1987, 1988 and 1989. Within the project: Fallout studies in the Gideå and Finnsjö areas after the Chernobyl accident in 1986
Thomas Ittner
SGAB, Uppsala
December 1990

TR 91-10
Sealing of rock joints by induced calcite precipitation. A case study from Bergeforsen hydro power plant
Eva Hakami[1], Anders Ekstav[2], Ulf Qvarfort[2]
[1]Vattenfall HydroPower AB
[2]Golder Geosystem AB
January 1991

TR 91-11
Impact from the disturbed zone on nuclide migration – a radioactive waste repository study
Akke Bengtsson[1], Bertil Grundfelt[1], Anders Markström[1], Anders Rasmuson[2]
[1]KEMAKTA Konsult AB
[2]Chalmers Institute of Technology
January 1991

TR 91-12
Numerical groundwater flow calculations at the Finnsjön site
Björn Lindbom, Anders Boghammar, Hans Lindberg, Jan Bjelkås
KEMAKTA Consultants Co, Stockholm
February 1991

TR 91-13
Discrete fracture modelling of the Finnsjön rock mass
Phase 1 feasibility study
J E Geier, C-L Axelsson
Golder Geosystem AB, Uppsala
March 1991

TR 91-14
Channel widths
Kai Palmqvist, Marianne Lindström
BERGAB-Berggeologiska Undersökningar AB
February 1991

TR 91-15
Uraninite alteration in an oxidizing environment and its relevance to the disposal of spent nuclear fuel
Robert Finch, Rodney Ewing
Department of Geology, University of New Mexico
December 1990

TR 91-16
Porosity, sorption and diffusivity data compiled for the SKB 91 study
Fredrik Brandberg, Kristina Skagius
Kemakta Consultants Co, Stockholm
April 1991

TR 91-17
Seismically deformed sediments in the Lansjärv area, Northern Sweden
Robert Lagerbäck
May 1991

TR 91-18
Numerical inversion of Laplace transforms using integration and convergence acceleration
Sven-Åke Gustafson
Rogaland University, Stavanger, Norway
May 1991

TR 91-19
NEAR21 - A near field radionuclide migration code for use with the PROPER package
Sven Norman[1], Nils Kjellbert[2]
[1]Starprog AB
[2]SKB AB
April 1991

TR 91-20
Äspö Hard Rock Laboratory. Overview of the investigations 1986-1990
R Stanfors, M Erlström, I Markström
June 1991

TR 91-21
Äspö Hard Rock Laboratory. Field investigation methodology and instruments used in the pre-investigation phase, 1986-1990
K-E Almén, O Zellman
June 1991

TR 91-22
Äspö Hard Rock Laboratory. Evaluation and conceptual modelling based on the pre-investigations 1986-1990
P Wikberg, G Gustafson, I Rhén, R Stanfors
June 1991

TR 91-23
Äspö Hard Rock Laboratory. Predictions prior to excavation and the process of their validation
Gunnar Gustafson, Magnus Liedholm, Ingvar Rhén, Roy Stanfors, Peter Wikberg
June 1991

TR 91-24
Hydrogeological conditions in the Finnsjön area. Compilation of data and conceptual model
Jan-Erik Andersson, Rune Nordqvist, Göran Nyberg, John Smellie, Sven Tirén
February 1991

TR 91-25
The role of the disturbed rock zone in radioactive waste repository safety and performance assessment. A topical discussion and international overview.
Anders Winberg
June 1991

TR 91-26
Testing of parameter averaging techniques for far-field migration calculations using FARF31 with varying velocity.
Akke Bengtsson[1], Anders Boghammar[1], Bertil Grundfelt[1], Anders Rasmuson[2]
[1]KEMAKTA Consultants Co
[2]Chalmers Institute of Technology

TR 91-27
Verification of HYDRASTAR. A code for stochastic continuum simulation of groundwater flow
Sven Norman
Starprog AB
July 1991

TR 91-28
Radionuclide content in surface and groundwater transformed into breakthrough curves. A Chernobyl fallout study in an forested area in Northern Sweden
Thomas Ittner, Erik Gustafsson, Rune Nordqvist
SGAB, Uppsala
June 1991

TR 91-29
Soil map, area and volume calculations in Orrmyrberget catchment basin at Gideå, Northern Sweden
Thomas Ittner, P-T Tammela, Erik Gustafsson
SGAB, Uppsala
June 1991

TR 91-30
A resistance network model for radionuclide transport into the near field surrounding a repository for nuclear waste (SKB, Near Field Model 91)
Lennart Nilsson, Luis Moreno, Ivars Neretnieks, Leonardo Romero
Department of Chemical Engineering,
Royal Institute of Technology, Stockholm
June 1991